Towards the Ultimate Conservative Difference Scheme V. A Second-order Sequel to Godunov's Method

Article *in* Journal of Computational Physics · July 1979

DOI: 10.1016/0021-9991(79)90145-1

CITATIONS
3,862

READS
979

1 author:

Bram van Leer
University of Michigan
198 PUBLICATIONS **15,746** CITATIONS

SEE PROFILE

JOURNAL OF COMPUTATIONAL PHYSICS 32, 101–136 (1979)

Towards the Ultimate Conservative Difference Scheme. V. A Second-Order Sequel to Godunov's Method

BRAM VAN LEER

University Observatory, Leiden, The Netherlands

Received October 18, 1977; revised October 17, 1978

A method of second-order accuracy is described for integrating the equations of ideal compressible flow. The method is based on the integral conservation laws and is dissipative, so that it can be used across shocks. The heart of the method is a one-dimensional Lagrangean scheme that may be regarded as a second-order sequel to Godunov's method. The second-order accuracy is achieved by taking the distributions of the state quantities inside a gas slab to be linear, rather than uniform as in Godunov's method. The Lagrangean results are remapped with least-squares accuracy onto the desired Euler grid in a separate step. Several monotonicity algorithms are applied to ensure positivity, monotonicity and nonlinear stability. Higher dimensions are covered through time splitting. Numerical results for one-dimensional and two-dimensional flows are presented, demonstrating the efficiency of the method. The paper concludes with a summary of the results of the whole series "Towards the Ultimate Conservative Difference Scheme."

1. INTRODUCTION

This paper describes a method of second-order accuracy for integrating the equations of ideal compressible flow (ICF). The method is based on the integral conservation laws and is dissipative, so that it can be used across shocks. The heart of the method is a one-dimensional Lagrangean scheme, the results of which are remapped onto the desired Euler grid in a separate step. Higher dimensions are covered through time splitting.

The Lagrangean scheme may be regarded as a second-order sequel to Godunov's [1] first-order Lagrangean scheme. As in the latter, the gas is divided into slabs, and the interaction of these slabs at their interfaces is considered in detail. Whereas in Godunov's method the distribution of the state quantities inside a slab are taken to be uniform, in the present method these distributions are taken to be linear. The information contained in the slopes of the distributions makes it possible to attain second-order accuracy in the method.

As in Godunov's method, the interaction of slabs is evaluated essentially on the basis of the characteristic equations, with due care taken to account for the discontinuities in the interaction flow. The convective difference scheme, hidden in the Lagrangean scheme, for integrating the characteristic equations is a so-called upstream-centered (upwind) scheme and has been discussed as "scheme II" in the pre-

0021-9991/79/070101–36$02.00/0

vious paper [2] of this series. Remapping the Lagrangean results onto an Euler grid is done according to the upstream-centered "scheme III" from the same paper. A substantial improvement will still result if, in the Lagrangean step, scheme II is replaced by the more accurate scheme III.

An accessory technique for preserving monotonicity during convection, also discussed in [2], is easily incorporated in the method. It is applied in its crudest form [2, Eq. (66)] at the beginning of the Lagrangean step; a more sophisticated form [2, Eq. (74)] is applied in the remap step. Further refinement of the technique has been projected.

Numerical experiments indicate that for solving two-dimensional flow problems, even on a coarse grid, the present second-order method is at least an order of magnitude more efficient than Godunov's method. An important reason for its efficiency is that the second-order method involves, per state quantity and per dimension, two independent data to describe the distribution in a slab (namely, the slab average and a representative slope value). This approach potentially has the effect of a mesh refinement of a factor two.

In solving two-dimensional flow problems on a conventional computer, the present method is 15–20% slower than another state-of-the-art method, namely, Phoenical Shasta FCT [3, 9]. The slight speed disadvantage seems to be amply offset by a greater accuracy. A detailed comparison with FCT and other algorithms may be published elsewhere [16].

Its efficiency aside, the most pleasant property of the present method is the clear physical picture associated with it. The discretization of initial values yields "real" gas slabs, with fully specified internal distributions of state quantities. The two basic aspects of fluid dynamics, conservation and (nonlinear) wave propagation are properly accounted for. The meaning of the various steps in the scheme is always evident, so that formulating boundary conditions and adding extra physics (radiation, multi-fluid) are straightforward. See also [2, Section 7] for a summary of the properties of the underlying convective scheme.

An all-purpose computer code for compressible gas dynamics, by the name of MUSCL (Monotonic Upstream-centered Scheme for Conservation Laws), was written along the above lines by P. R. Woodward at Leiden Observatory. Various improvements are presently being installed by him at Lawrence Livermore Laboratory.

The present paper is built up as follows. The physical, mathematical and numerical aspects of the Lagrangean scheme are treated in Section 2, while the extra features needed to incorporate the scheme into a monotonic multi-dimensional Eulerian method are presented in Section 3. Numerical results for shock tube flow and for supersonic flow in a windtunnel with a step, obtained with MUSCL and with Godunov's method, are displayed and compared in Section 4. The conclusions from the present paper and, more generally, from the series "Towards the Ultimate Conservative Difference Scheme" are given in Section 5, together with a list of desirable further developments. Finally, Appendix A adds some mathematical and numerical support to the earlier discussion of the interaction of gas slabs, while Appendix B discusses various ways to find a representative slope value for a distribution inside a slab.

2. The Lagrangean Scheme

2.1. *The Lagrangean Flow Equations*

As the main building block of the method is a one-dimensional Lagrangean scheme, I shall first discuss the Lagrangean equations of ICF in one dimension. These read

$$\partial V/\partial t - \partial(x^\alpha u)/\partial \xi = 0, \tag{1}$$

$$\partial u/\partial t + x^\alpha \, \partial p/\partial \xi = F, \tag{2}$$

$$\partial E/\partial t + \partial(x^\alpha up)/\partial \xi = uF + G, \tag{3}$$

$$\partial x/\partial t = u. \tag{4}$$

Here the independent variables are the time t and the mass coordinate ξ; the latter is coupled to the gas and relates to the space coordinate x and the volume coordinate X by

$$d\xi = V^{-1}x^\alpha \, dx = V^{-1}d\{x^{\alpha+1}/(\alpha + 1)\} \equiv V^{-1} \, dX. \tag{5}$$

For $\alpha = 0$, 1 or 2 we have plane, cylindrical or spherical symmetry, respectively.

The state quantities V, u, E and p are, respectively, specific volume, velocity, specific total energy and pressure. Denoting the specific internal energy by e we have

$$E = e + \tfrac{1}{2}u^2. \tag{6}$$

The equation of state will be written as

$$p \equiv p(V, e). \tag{7}$$

Where further specification is desired, the ideal gas law will be used:

$$p = (\gamma - 1)\, e/V. \tag{8γ}$$

Here γ represents the ratio of specific heats. Formulas into which this equation of state has been inserted will be distinguished from formulas valid for any equation of state by a "γ" following the formula number. If the equation of state is more complicated, it may nevertheless be approximated by Eq. (8γ) using an effective value of γ per gas slab and per time step.

The quantities F and G represent sources of momentum and internal energy and may be functions of all independent and dependent variables, including those related to the other space dimensions. If specification is needed, dependence on V, u, E and x will be assumed.

Eq. (2) may be written as

$$\partial u/\partial t + \partial(x^\alpha p)/\partial \xi = \alpha V p/x + F, \tag{9}$$

to make it look more like Eqs. (1) and (3). Eq. (4) may be written as

$$\partial X/\partial t = x^{\alpha}u, \tag{10}$$

to bring out that Eq. (1) derives from it through differentiation with respect to ξ.

An important state quantity is the Lagrangean sound speed C (mass in column of unit cross-section travelled per unit time), defined by

$$C^2 \equiv -(\partial p/\partial V)_{\text{adiabatic}} \tag{12}$$

and related to the spatial sound speed c by

$$C = c/V. \tag{13}$$

For an ideal gas we have

$$C^2 = \gamma p/V. \tag{14}\gamma$$

Combining Eqs. (1)–(3) with the definition of C leads us to the characteristic equations

$$\partial p/\partial t + C^2\,\partial V/\partial t = G(\partial p/\partial e)_V\,, \tag{15}$$

$$\begin{aligned}(\partial u/\partial t - C^{-1}\,\partial p/\partial t) - x^{\alpha}C(\partial u/\partial \xi - C^{-1}\,\partial p/\partial \xi)\\ = \alpha uVC/x + F - C^{-1}G(\partial p/\partial e)_V\,,\end{aligned} \tag{18}$$

$$\begin{aligned}(\partial u/\partial t + C^{-1}\,\partial p/\partial t) + x^{\alpha}C(\partial u/\partial \xi + C^{-1}\,\partial p/\partial \xi)\\ = -\alpha uVC/x + F + C^{-1}G(\partial p/\partial e)_V\,.\end{aligned} \tag{19}$$

The quantity $(\partial p/\partial e)_V$, evaluated on the basis of the ideal gas law, becomes

$$(\partial p/\partial e)_V = (\gamma - 1)/V. \tag{17}\gamma$$

Introducing the Riemann invariants J^- and J^+, and the entropy S (apart from an integrating factor) we may write Eqs. (18), (19) and (15) as

$$\begin{aligned}dJ^- \equiv du - C^{-1}\,dp = \{\alpha uVC/x + F - C^{-1}G(\partial p/\partial e)_V\}\,dt\\ \text{on a trajectory with } d\xi/dt = -x^{\alpha}C,\end{aligned} \tag{20}$$

$$\begin{aligned}dJ^+ \equiv du + C^{-1}\,dp = \{-\alpha uVC/x + F + C^{-1}G(\partial p/\partial e)_V\}\,dt\\ \text{on a trajectory with } d\xi/dt = +x^{\alpha}C,\end{aligned} \tag{21}$$

$$\begin{aligned}dS \sim dp + C^2\,dV = G(\partial p/\partial e)_V\,dt\\ \text{on a trajectory with } d\xi/dt = 0.\end{aligned} \tag{22}$$

The trajectories on which Eqs. (20) and (21) hold will be called the Γ^- and Γ^+ characteristics, respectively; the trajectory on which Eq. (22) holds is a streamline. Using the ideal gas law, Eq. (22) can be integrated to

$$(pV^{\gamma})_t = (pV^{\gamma})_{t^0} \exp\left\{\int_{t^0}^{t} (G/e)\,dt'\right\} \quad \text{on a streamline.} \tag{23}\gamma$$

Across a shock wave, none of the flow equations in differential form holds. From the integral form of the conservation laws (1), (9) and (3) the following jump equations can be derived:

$$\pm W(V^* - V) + (u^* - u) = 0, \tag{24}$$

$$\pm W(u^* - u) - (p^* - p) = 0, \tag{25}$$

$$\pm W(E^* - E) - (u^*p^* - up) = 0. \tag{26}$$

Post-shock values are indicated by an asterisk; the Lagrangean shock speed is called $\pm W$, where W is positive and the sign indicates the direction of propagation. This shock speed, like the Lagrangean sound speed, is defined as the mass flux through the wave in a column of unit cross-section, and does not include the geometrical factor x^α. To find the spatial speed with respect to the gas, W must be multiplied by the pre-shock specific volume V.

In view of numerical applications it is useful to derive an expression for W in which only one post-shock value appears. A practical choice is

$$W = C[1 + \{(\gamma + 1)/(2\gamma)\}(p^* - p)/p]^{1/2}, \qquad p^* \geqslant p. \tag{31γ}$$

For a centered rarefaction wave connecting two uniform and constant states we have

$$(u^* - u) \mp \{2/(\gamma - 1)\}(V^*C^* - VC) = 0 \tag{32γ}$$

across a wave moving to the right/left; furthermore,

$$p^*V^{*\gamma} = pV^\gamma. \tag{33γ}$$

From these relations one may obtain pseudo-jump equations similar to (24)-(26); however, the wave speeds appearing in those equations are all different. We shall only use the equivalent of Eq. (25); for a rarefaction fan we arrive at the effective Lagrangean speed

$$W = \left| \frac{p^* - p}{u^* - u} \right| = \frac{\gamma - 1}{2\gamma} \frac{1 - p^*/p}{1 - (p^*/p)^{(\gamma-1)/(2\gamma)}} C, \qquad p^* < p. \tag{34γ}$$

If the states connected by the wave are not uniform or constant, Eqs. (32γ)-(34γ) are only meaningful in computing the effective wave speed in the divergence center of the rarefaction fan.

From the symmetric appearance of pre- and post-wave states in the (pseudo) jump equations it follows, for sufficiently weak waves, that

$$W = \tfrac{1}{2}(C + C^*) + O\{(C^* - C)^2\}, \tag{35}$$

regardless of the type of wave and the equation of state. For infinitesimally weak waves the wave speed W reduces, of course, to the sound speed C. It follows from Eq. (25) that

$$| dp^*/du^* |_{(u,p)} = C. \tag{38}$$

2.2. *Discretization*

The gas is divided into slabs that need not have equal thickness $\Delta\xi$. Values taken at the interfaces will bear an integer index; values taken in the middle of a slab and values averaged over a slab (the latter distinguished by an overhead bar) will bear a half-integer index. In order to suppress the time index, initial values and values averaged over a time step (the latter distinguished by angled brackets around them) are denoted by writing the space index as a superscript. The complete notation has been compiled in Table I.

TABLE I

Notation Used in the Grid

Symbol	Definition
ξ_i, x_i, X_i	mass, Euler, volume coordinate of zone boundary
$\bar{\xi}_{i+1/2}$	$\frac{1}{2}(\xi_i + \xi_{i+1})$, mass-averaged mass coordinate of zone (ξ_i, ξ_{i+1})
$\bar{X}_{i+1/2}$	$\frac{1}{2}(X_i + X_{i+1})$, volume-averaged volume coordinate of zone (X_i, X_{i+1})
$\Delta_{i+1/2}\xi$, $\Delta_{i+1/2}X$	$\xi_{i+1} - \xi_i$, $X_{i+1} - X_i$
t^0	Initial time level
t^1	$t^0 + \Delta t$, final time level
$\bar{Q}_{i+1/2}$, $\bar{Q}^{i+1/2}$	Mass-averaged value of Q in zone (ξ_i, ξ_{i+1}) at t^0, t^1
$\tilde{Q}_{i+1/2}$, $\tilde{Q}^{i+1/2}$	Volume-averaged value of Q in zone (x_i, x_{i+1}) at t^0, t^1
Q_i, Q^i	Value of Q at the boundary ξ_i at t^0, t^1
$\langle Q\rangle_i$	Average value of Q at the boundary ξ_i during time step
$\langle\bar{Q}\rangle_{i+1/2}$	Average value of $\bar{Q}$ in zone (ξ_i, ξ_{i+1}) during time step
$\Delta_i\bar{Q}$, $\Delta^i\bar{Q}$	$\bar{Q}_{i+1/2} - \bar{Q}_{i-1/2}$, $\bar{Q}^{i+1/2} - \bar{Q}^{i-1/2}$
$\bar{\Delta}_{i+1/2}Q/\Delta_{i+1/2}\xi$	Mass-averaged value of $\partial Q/\partial\xi$ in zone (ξ_i, ξ_{i+1}) at t^0
$\tilde{\Delta}_{i+1/2}Q/\Delta_{i+1/2}X$	Volume-averaged value of $\partial Q/\partial X$ in zone (X_i, X_{i+1}) at t^0

In each slab we shall, at the initial level t^0 of a time step, approximate the true initial-value distributions of the conserved quantities V, u and E by linear distributions with the correct slab integral. For instance, the distribution of V is approximated by

$$\{V(t^0, \xi)\}_{\text{approx}} = \bar{V}_{i+1/2} + (\bar{\Delta}_{i+1/2}V/\Delta_{i+1/2}\xi)(\xi - \bar{\xi}_{i+1/2}),\ \xi_i < \xi < \xi_{i+1}, \tag{39}$$

in which the slab average is defined by

$$\bar{V}_{i+1/2} \equiv (\Delta_{i+1/2}\xi)^{-1}\int_{\xi_i}^{\xi_{i+1}} V(t^0, \xi)\, d\xi \tag{40}$$

and the average slope as

$$\begin{aligned}\bar{\Delta}_{i+1/2}V/\Delta_{i+1/2}\xi &\equiv \overline{\{\partial V(t^0, \xi)/\partial\xi\}}_{i+1/2} \equiv (\Delta_{i+1/2}\xi)^{-1}\int_{\xi_i}^{\xi_{i+1}} \frac{\partial}{\partial\xi} V(t^0, \xi)\, d\xi \\ &\equiv \Delta_{i+1/2}V(t^0, \xi)/\Delta_{i+1/2}\xi.\end{aligned} \tag{41}$$

The above way of finding a representative slope value will be called interface differencing. This must however be regarded as a temporary substite for the more accurate least-squares fitting, which is used in the Eulerian remap step (see Sec. 3.2). To date, a practical way of updating a slope with least-squares accuracy in the Lagrangean step has not yet been found. The pros and cons of various ways of defining the slopes are discussed in Appendix B with special regard to the equations of ICF; see also [2, Sec. 2].

The six quantities $\bar{V}$, $\bar{u}$, $\bar{E}$, $\bar{\Delta}V$, $\bar{\Delta}u$ and $\bar{\Delta}E$ are the only data on the true initial values of V, u and E inside a slab that are retained and, in consequence, are updated in the next time step. In addition, the Euler coordinate x or the volume coordinate X of each slab boundary is integrated along. From Eqs. (5) and (40) it follows that

$$\Delta_{i+1/2}X = \bar{V}_{i+1/2}\Delta_{i+1/2}\xi. \tag{42}$$

A linear distribution of E is not very useful in itself, except in remapping total energy onto an Eulerian grid (see Sec. 3.2). In the Lagrangean scheme it is more convenient to work with a linear *pressure* distribution instead. Using the available discrete information, the average pressure and pressure gradient may be recovered within $O\{(\Delta\xi)^4\}$ and $O\{(\Delta\xi)^2\}$, respectively. We first obtain

$$\bar{e}_{i+1/2} = \bar{E}_{i+1/2} - \frac{1}{2}\left(\bar{u}^2_{i+1/2} + \frac{1}{12}(\bar{\Delta}_{i+1/2}u)^2\right) + O\{(\Delta\xi)^4\}, \tag{43}$$

$$\bar{\Delta}_{i+1/2}e = \bar{\Delta}_{i+1/2}E - \bar{u}_{i+1/2}\bar{\Delta}_{i+1/2}u + O\{(\Delta\xi)^3\}, \tag{44}$$

and then, with aid of the ideal gas law,

$$\bar{\Delta}_{i+1/2}p = p(\bar{V}_{i+1/2}, \bar{e}_{i+1/2})(\bar{\Delta}_{i+1/2}e/\bar{e}_{i+1/2} - \bar{\Delta}_{i+1/2}V/\bar{V}_{i+1/2}) + O\{(\Delta\xi)^3\}, \tag{45γ}$$

$$\bar{p}_{i+1/2} = p(\bar{V}_{i+1/2}, \bar{e}_{i+1/2}) - \frac{1}{12}(\bar{\Delta}_{i+1/2}V/\bar{V}_{i+1/2})\,\bar{\Delta}_{i+1/2}p + O\{(\Delta\xi)^4\}. \tag{46γ}$$

However, the dependence of $\bar{e}$ and $\bar{p}$, as approximated above, on $\bar{\Delta}V$, $\bar{\Delta}u$ and $\bar{\Delta}E$ in practice is a nuisance. For instance, it makes the otherwise explicit monotonicity algorithm of Sec. 3.3 implicit for the pressure. We shall therefore make no use of Eqs. (43) and (46γ) but, instead, employ the sufficiently accurate formulas

$$\bar{e}_{i+1/2} = \bar{E}_{i+1/2} - \tfrac{1}{2}\bar{u}^2_{i+1/2} + O\{(\Delta\xi)^2\}, \tag{47}$$

$$\bar{p}_{i+1/2} = p(\bar{V}_{i+1/2}, \bar{e}_{i+1/2}) + O\{(\Delta\xi)^2\}. \tag{48}$$

Note that the slope values are independent of the slab averages; they can not be derived from the latter and must be stored separately. This is one of the features that distinguishes the present scheme from common finite-difference schemes. The difference with Godunov's scheme is that, in the latter, all slopes are taken to be zero. This accounts for the first-order accuracy of Godunov's scheme; see also [2, Sec. 2]. A short discussion of Godunov's method can be found, for instance, in [19].

Exact formulas for updating the slab averages of the conserved quantities result from integrating the conservation laws (1), (9), (3) over a slab and a time step:

$$\bar{V}^{i+1/2} = \bar{V}_{i+1/2} + \frac{\Delta t}{\Delta_{i+1/2}\xi}(\langle x^\alpha u\rangle_{i+1} - \langle x^\alpha u\rangle_i), \tag{49}$$

$$\bar{u}^{i+1/2} = \bar{u}_{i+1/2} - \frac{\Delta t}{\Delta_{i+1/2}\xi}(\langle x^\alpha p\rangle_{i+1} - \langle x^\alpha p\rangle_i) + (\langle \overline{\alpha p V/x}\rangle_{i+1/2} + \langle \bar{F}\rangle_{i+1/2})\,\Delta t, \tag{50}$$

$$\bar{E}^{i+1/2} = \bar{E}_{i+1/2} - \frac{\Delta t}{\Delta_{i+1/2}\xi}(\langle x^\alpha up\rangle_{i+1} - \langle x^\alpha up\rangle_i) + (\langle \overline{uF}\rangle_{i+1/2} + \langle \bar{G}\rangle_{i+1/2})\,\Delta t; \tag{51}$$

these hold regardless of the presence of discontinuities in the slab. As usual in control-volume schemes, for updating $\bar{V}$, $\bar{u}$ and $\bar{E}$ we need to estimate the time averages $\langle u\rangle$, $\langle p\rangle$ and $\langle x\rangle$ of velocity, pressure and Euler coordinate at each interface with first-order accuracy, that is, within a margin of $O\{(\Delta t)^2\}$. Time averages of products of these quantities may be approximated by products of their time averages.

For updating $\bar{\Delta}V$, $\bar{\Delta}u$ and $\bar{\Delta}p$ we must estimate, with the same accuracy, interface values of V, u and p at the final time level t^1 and take their differences; for example:

$$\Delta^{i+1/2}V = V^{i+1} - V^i. \tag{51.5}$$

The particular manner of computing the flow at the interfaces is another distinguishing property of the present integration scheme and will be discussed in the next section.

The Euler coordinate of an interface is updated according to

$$x^i = x_i + \langle u\rangle_i\,\Delta t, \tag{52}$$

from which follows the volume coordinate X^i. It is seen from Eq. (10) that updating $\bar{V}$ according to

$$\bar{V}^{i+1/2} = \Delta^{i+1/2}X/\Delta_{i+1/2}\xi \tag{53}$$

is equivalent to using Eq. (49). In practice, Eq. (53) is preferred to Eq. (49).

2.3. *Interaction of Slabs*

After discretization the initial-value distributions in the slabs (ξ_{i-1}, ξ_i) and (ξ_i, ξ_{i+1}) generally meet, at ξ_i, in a discontinuity. Denoting values at the left and the right side of the interface by the indices i_- and i_+, respectively, we have

$$V_{i\pm} = \bar{V}_{i\pm1/2} \mp \tfrac{1}{2}\bar{\Delta}_{i\pm1/2}V, \tag{54}$$

$$u_{i\pm} = \bar{u}_{i\pm1/2} \mp \tfrac{1}{2}\bar{\Delta}_{i\pm1/2}u, \tag{55}$$

$$p_{i\pm} = \bar{p}_{i\pm1/2} \mp \tfrac{1}{2}\bar{\Delta}_{i\pm1/2}p. \tag{56}$$

From these follow all other state quantities needed, in particular $C_{i\pm}$.

The discontinuity will exist only for a time-interval with zero measure, so that the above initial values will not contribute to the time averages $\langle u\rangle_i$, $\langle p\rangle_i$ and $\langle x\rangle_i$ needed in our scheme. In determining what happens at ξ_i during the next step in time we must start with resolving the initial discontinuity. Once resolved, the state at ξ_i will continue to change, because the interacting slabs generally are not uniform and because geometric effects and sources may enter. Knowledge only of the first time derivatives of velocity, pressure and specific volume, arising at ξ_i immediately after the resolution, will enable us to calculate the evolution of all state quantities at the interface within the desired margin of $O\{(\Delta t)^2\}$.

As is well known, an arbitrary fluid discontinuity will break up into a pair of waves, one running to the left and one running to the right. Each of these may be a shock wave or a rarefaction wave. In between the waves, velocity and pressure are continuous; the specific volume generally is still discontinuous at the interface.

We may describe the state resulting immediately after resolution of the initial discontinuity with aid of the equations for jumps and wave speeds given in Section 2.1. By virtue of Eq. (25) we have

$$W_{i-}(u_i^* - u_{i-}) + (p_i^* - p_{i-}) = 0, \tag{57}$$

$$W_{i+}(u_i^* - u_{i+}) - (p_i^* - p_{i+}) = 0. \tag{58}$$

Here u_i^* and p_i^* are the resulting values of u and p in ξ_i, while W_{i-} and W_{i+} are the absolute values of the speeds of the waves travelling into the slabs (ξ_{i-1}, ξ_i) and (ξ_i, ξ_{i+1}), respectively. Eliminating u_i^* from these equations yields

$$p_i^* = \{W_{i+}p_{i-} + W_{i-}p_{i+} - W_{i-}W_{i+}(u_{i+} - u_{i-})\}/(W_{i-} + W_{i+}). \tag{59}$$

Since W_{i-} and W_{i+} can be expressed, according to Eqs. (31γ) and (34γ), in terms of p_i^* and the known quantities $p_{i\mp}$ and $C_{i\mp}$, the resolved pressure value is, in principle, determined. In practice, p_i^* is obtained through an iterative procedure, using

$$p_i^{*(1)} = \{(C_{i+}p_{i-} + C_{i-}p_{i+} - C_{i-}C_{i+}(u_{i+} - u_{i-})\}/(C_{i-} + C_{i+}) \tag{60}$$

as a starting value.

After satisfactory convergence of the pressure values, u_i^* is determined from

$$u_i^* = \{W_{i-}u_{i-} + W_{i+}u_{i+} - (p_{i+} - p_{i-})\}/(W_{i-} + W_{i+}), \tag{61}$$

an equation that results when p_i^* is eliminated from Eqs. (57) and (58). The values V_{i-}^* and V_{i+}^* of the specific volume on the left and the right side of the contact discontinuity, resulting at ξ_i immediately after resolution of the initial discontinuity, are obtained with aid of either Eq. (24) or Eq. (33γ), depending on the kind of wave appearing on either side. The resolved state is then completely determined.

Godunov's own iterative procedure for obtaining p_i^* brings the pressure a factor $O\{(u_{i+} - u_{i-}), (p_{i+} - p_{i-})\}$ closer to the exact value, per iteration cycle. I have abandoned Godunov's procedure for a more efficient one, advancing a factor

$O\{(u_{i+} - u_{i-})^2, (p_{i+} - p_{i-})^2\}$ in accuracy per cycle. Both procedures are explained further in Appendix A on the basis of pressure-versus-velocity diagrams.

It must be understood that, when calculating smooth flow in a uniform grid with the present method, the size of the discontinuities is of the order $O\{(\Delta\xi)^3\}$, as opposed to $O(\Delta\xi)$ in Godunov's method. The accuracy required at the interfaces is only $O\{(\Delta t)^2\}$. In consequence, *even* $p_i^{*(1)}$, *with an error* $O\{(C_\pm^* - C_\pm)[(p_+ - p_-), (u_+ - u_-)]\} \sim O\{(\Delta\xi)^6\}$ *is more than adequate to serve as* p_i^* *anywhere in the smooth part of the flow.*

The corresponding value of u_i^* is

$$u_i^{*(1)} = \{C_{i-}u_{i-} + C_{i+}u_{i+} - (p_{i+} - p_{i-})\}/(C_{i-} + C_{i+}), \tag{62}$$

while $V_{i\pm}^{*(1)}$ follows from

$$\pm C_{i\pm}(V_{i\pm}^{*(1)} - V_{i\pm}) + (u_i^{*(1)} - u_{i\pm}) = 0. \tag{63}$$

Using Eqs. (60), (62) and (63) implies interaction of the slabs through linear waves, since the difference between $W_{i\pm}$ and $C_{i\pm}$ is ignored. This approximation obviously breaks down at interfaces lying inside a shock structure. The penalty for using a bad estimate of u_i^* and p_i^* in such places is the enhancement of numerical oscillations in the post-shock region, an effect also known for Godunov's method. In the MUSCL code, therefore, the iterations are called for if $p_i^{*(1)}$ differs more than 1 % from $p_{i\pm1}$ and are continued until $p_i^{*(n)}$ does not differ more than 1.5 % from $p_i^{*(n-1)}$; this appears to be satisfactory. In the exploding-diaphragm calculation of Sec. 4, the extra iteration. in selected points accounted for 2-3 % of the computing time of the Lagrangean step.

In view of the low accuracy required beyond the linear-interaction formulas it even seems wasteful to use, in the iterations, the exact wave speed formulas (31γ) and (34γ). We may as well take one approximate formula that does not distinguish between the shock and rarefaction cases, such as Eq. (35). This possibility is presently in study. Note that using such approximate physics does not mean that the scheme for updating slab *averages* can not distinguish between a shock wave and a rarefaction wave. As long as the scheme is consistent, stable, conservative and irreversible in time, it will raise the entropy in a slab where necessary.

The time derivatives $(\partial u/\partial t)_i^*$, $(\partial p/\partial t)_i^*$ and $(\partial V/\partial t)_{i\pm}^*$ of the resolved state at ξ_i are determined essentially from the characteristic equations (18), (19) and (15). At interfaces where one or more extra iterations were needed for the resolution, we use the following version of Eqs. (18) and (19), valid at a discontinuity:

$$\left(\frac{\partial u}{\partial t}\right)_i - \frac{1}{C_{i+}^*}\left(\frac{\partial p}{\partial t}\right)_i^* - x_i^\alpha W_{i+}\left(\frac{\partial u}{\partial \xi} - \frac{1}{C}\frac{\partial p}{\partial \xi}\right)_{i+} = -x_i^\alpha\left(\frac{V^* - V}{4V}\right)_{i+}\left(\frac{\partial p}{\partial \xi} + C^2\frac{\partial V}{\partial \xi}\right)_{i+}$$

$$+ \frac{\alpha}{x_i}\left\{\frac{C}{2W}(uVC + u^*V^*C^*)\right\}_{i+} + \tfrac{1}{2}(F + F^*)_{i+}$$

$$- \left[\frac{C}{2W}\left\{\frac{G}{C}\left(\frac{\partial p}{\partial e}\right)_V + \frac{G^*}{C^*}\left(\frac{\partial p}{\partial e}\right)_V^*\right\}\right]_{i+} + O\{(C^* - C)_{i+}^2\}, \tag{64}$$

$$\left(\frac{\partial u}{\partial t}\right)_i^* + \frac{1}{C_{i-}^*}\left(\frac{\partial p}{\partial t}\right)_i^* + x_i{}^\alpha W_{i-}\left(\frac{\partial u}{\partial \xi} + \frac{1}{C}\frac{\partial p}{\partial \xi}\right)_{i-} = -x_i{}^\alpha\left(\frac{V^* - V}{4V}\right]_{i-}\left(\frac{\partial p}{\partial \xi} + C^2\frac{\partial V}{\partial \xi}\right)_{i-}$$

$$- \frac{\alpha}{x_i}\left\{\frac{C}{2W}(uVC + u^*V^*C^*)\right\}_{i-} + \tfrac{1}{2}(F + F^*)_{i-}$$

$$+ \left[\frac{C}{2W}\left\{\frac{G}{C}\left(\frac{\partial p}{\partial e}\right)_V + \frac{G^*}{C^*}\left(\frac{\partial p}{\partial e}\right)_V^*\right\}\right]_{i-} + O\{(C^* - C)_{i-}^2\}, \tag{65}$$

These equations, like Eq. (35), distinguish between C and W, but not between a shock wave and a rarefaction wave. They were derived in [17]. Eq. (15), applied to the resolved state on either side of ξ_i, reads:

$$\left(\frac{\partial p}{\partial t}\right)_i^* + \left(C^2\frac{\partial V}{\partial t}\right)_{i\pm}^* = \left\{G\left(\frac{\partial p}{\partial e}\right)_V\right\}_{i\pm}^*. \tag{66}$$

In Eqs. (64)-(66) the space derivatives on either side of ξ_i, indicated by the subscript $i_\pm$, numerically are equal to the average space derivatives in the slabs that meet in ξ_i. This is consistent with the piecewise-linear representation of initial values.

At interfaces where no extra iterations were used for the resolution, the differences between C and W and between quantities with and without asterisk may be ignored in the coefficients and source terms in Eqs. (64)-(66).

The time derivatives given by Eqs. (64)-(66) can be used to describe the evolution of V, u and p at ξ_i until the waves from ξ_{i-1} and/or ξ_{i+1} arrive at ξ_i. This implies the usual Courant condition on the time step.

Using Eqs. (57), (58), (64) and (65) to calculate the flow at an interface guarantees that signals coming from the left-hand and from the right-hand side are properly separated. It is easily checked that the slab averages of the Riemann invariants J^- and J^+ are updated by the Lagrangean scheme according to a second-order *upstream-centered* (upwind) difference formula resembling Fromm's [11] scheme for integrating the convection equation. Convective schemes of this type were discussed in [2].

2.4. *Details of the Lagrangean Scheme*

In each slab at t^0 we are given the quantities $\overline{V}$, $\bar{u}$, $\bar{E}$, $\overline{\Delta V}$, $\overline{\Delta u}$ and $\overline{\Delta E}$ (if the last step was an Eulerian remap) or $\overline{\Delta p}$ (if the last step was Lagrangean). At the interfaces we are given ξ (constant during a Lagrangean step) and x; from the latter we obtain X (see Eq. (5)). In each slab we further obtain $\bar{p}$ and (if not already given) $\overline{\Delta p}$ according to Eqs. (47), (48), (44) and (45γ). While calculating $\bar{p}$ we may locally check the Lagrangean Courant condition on Δt,

$$\Delta t \leqslant (\Delta x)/\bar{c}, \tag{67}$$

or, if $\bar{c}$ itself is not needed for other reasons,

$$\gamma(\gamma - 1)(\Delta t)^2 \leqslant (\Delta x)^2/\bar{e}, \tag{68γ}$$

avoiding a square-root computation in each slab (see Eqs. (12), (13)). After a safe value of Δt has been established for the whole grid, which may be multi-dimensional, we may proceed with steps that are exclusively one-dimensional.

At each interface we first compute the values of $V_\pm$, $u_\pm$ and $p_\pm$ according to Eqs. (54)-(56), from which follow the values of $C_\pm$, $(\partial p/\partial e)_\pm$, $F_\pm$ and $G_\pm$. Next, the discontinuities at the interfaces are resolved as described in Sec. 2.3, yielding values of u^*, p^*, $W_\pm$ and $V_\pm^*$. From these, if necessary, are derived $C_\pm^*$, $(\partial p/\partial e)_\pm^*$, $F_\pm^*$ and $G_\pm^*$. We now know all quantities occurring in Eqs. (64)-(66) except $(\partial u/\partial t)^*$, $(\partial p/\partial t)^*$ and $(\partial V/\partial t)_\pm^*$. Subtracting Eq. (64) from Eq. (65) eliminates $(\partial u/\partial t)^*$, yielding $(\partial p/\partial t)^*$. Adding up C_+^* times Eq. (64) and C_-^* times Eq. (65) eliminates $(\partial p/\partial t)^*$, yielding $(\partial u/\partial t)^*$. Inserting $(\partial p/\partial t)^*$ into Eq. (66) then yields $(\partial V/\partial t)_\pm^*$.

The scheme then proceeds with a half step in time, defined by the following equations:

$$\langle V\rangle_{i\pm} = V_{i\pm}^* + \tfrac{1}{2}(\partial V/\partial t)_{i\pm}^*\,\Delta t + O\{(\Delta t)^2\}, \tag{69}$$

$$\langle u\rangle_i = u_i^* + \tfrac{1}{2}(\partial u/\partial t)_i^*\,\Delta t + O\{(\Delta t)^2\}, \tag{70}$$

$$\langle p\rangle_i = p_i^* + \tfrac{1}{2}(\partial p/\partial t)_i^*\,\Delta t + O\{(\Delta t)^2\}, \tag{71}$$

$$\langle x\rangle_i = x_i + \tfrac{1}{2}u_i^*\,\Delta t + O\{(\Delta t)^2\}, \tag{72}$$

$$\langle x^\alpha\rangle_i = \langle x\rangle_i^\alpha + O\{(\Delta t)^2\}, \tag{73}$$

$$\langle \bar V\rangle_{i+1/2} = \tfrac{1}{2}(\langle V\rangle_{i+} + \langle V\rangle_{(i+1)-}) + O\{(\Delta t)^2, (\Delta\xi)^2\}, \tag{74}$$

$$\langle \bar u\rangle_{i+1/2} = \tfrac{1}{2}(\langle u\rangle_i + \langle u\rangle_{i+1}) + O\{(\Delta t)^2, (\Delta\xi)^2\}, \tag{75}$$

$$\langle \bar p\rangle_{i+1/2} = \tfrac{1}{2}(\langle p\rangle_i + \langle p\rangle_{i+1}) + O\{(\Delta t)^2, (\Delta\xi)^2\}, \tag{76}$$

$$\langle \bar x\rangle_{i+1/2} = \tfrac{1}{2}(\langle x\rangle_i + \langle x\rangle_{i+1}) + O\{(\Delta t)^2, (\Delta\xi)^2\}, \tag{77}$$

$$\langle \bar F\rangle_{i+1/2} = F(\langle \bar V\rangle_{i+1/2}, \langle \bar u\rangle_{i+1/2}, \langle \bar p\rangle_{i+1/2}, \langle \bar x\rangle_{i+1/2}) + O\{(\Delta t)^2, (\Delta\xi)^2\}, \tag{78}$$

$$\langle \bar G\rangle_{i+1/2} = G(\langle \bar V\rangle_{i+1/2}, \langle \bar u\rangle_{i+1/2}, \langle \bar p\rangle_{i+1/2}, \langle \bar x\rangle_{i+1/2}) + O\{(\Delta t)^2, (\Delta\xi)^2\}. \tag{79}$$

The full time step, modeled after Eqs. (50)-(53), can now be carried out with the proper accuracy:

$$x^i = x_i + \langle u\rangle_i\,\Delta t + O\{(\Delta t)^3\}, \tag{80}$$

$$X^i = (x^i)^{\alpha+1}/(\alpha+1), \tag{81}$$

$$\bar V^{i+1/2} = \Delta^{i+1/2}X/\Delta_{i+1/2}\xi, \tag{82}$$

$$\bar u^{i+1/2} = \bar u_{i+1/2} - \frac{\Delta t}{\Delta_{i+1/2}\xi}\,[\Delta_{i+1/2}(\langle x^\alpha\rangle\langle p\rangle) - \langle \bar p\rangle_{i+1/2}\,\Delta_{i+1/2}\langle x^\alpha\rangle] + \langle \bar F\rangle_{i+1/2}\,\Delta t + O\{(\Delta t)^3, \Delta t(\Delta\xi)^2\}, \tag{83}$$

$$\bar{E}^{i+1/2} = \bar{E}_{i+1/2} - \frac{\Delta t}{\Delta_{i+1/2}\xi}\,\Delta_{i+1/2}(\langle x^\alpha\rangle\langle u\rangle\langle p\rangle)$$

$$+ (\langle\bar{u}\rangle_{i+1/2}\langle\bar{F}\rangle_{i+1/2} + \langle\bar{G}\rangle_{i+1/2})\,\Delta t + O\{(\Delta t)^3, \Delta t(\Delta\xi)^2\}, \tag{84}$$

$$V^{i\pm} = V^*_{i\pm} + (\partial V/\partial t)^*_{i\pm}\,\Delta t + O\{(\Delta t)^2\}, \tag{85}$$

$$u^i = u^*_i + (\partial u/\partial t)^*_i\,\Delta t + O\{(\Delta t)^2\}, \tag{86}$$

$$p^i = p^*_i + (\partial p/\partial t)^*_i\,\Delta t + O\{(\Delta t)^2\}, \tag{87}$$

$$\bar{\Delta}^{i+1/2}V = V^{(i+1)-} - V^{i+} + O\{(\Delta t)^2\,\Delta\xi\}, \tag{88}$$

$$\bar{\Delta}^{i+1/2}u = u^{i+1} - u^i + O\{(\Delta t)^2\,\Delta\xi\}, \tag{89}$$

$$\bar{\Delta}^{i+1/2}p = p^{i+1} - p^i + O\{(\Delta t)^2\,\Delta\xi\}. \tag{90}$$

If the Lagrangean step is followed by an Eulerian remap, $\bar{\Delta}p$ must be converted back into $\bar{\Delta}E$ using Eqs. (47) and (48) and, inversely, Eqs. (45γ) and (44).

The term in Eq. (83) between square brackets is identical to $\langle\overline{x^\alpha}\rangle_{i+1/2}\,\Delta_{i+1/2}\langle p\rangle$ (compare Eq. (2)), with $\langle\overline{x^\alpha}\rangle_{i+1/2}$ defined as $\frac{1}{2}(\langle x^\alpha\rangle_i + \langle x^\alpha\rangle_{i+1})$, but avoids introducing the latter quantity. The time averages $\langle x\rangle_i$ and $\langle x^\alpha\rangle_i$ may be calculated up to $O\{(\Delta t)^3\}$, using $(\partial^2 x/\partial t^2)_i \equiv (\partial u/\partial t)^*_i$. The calculation of the time- and space-averaged source terms may also be varied. The steps listed above just form the bare-minimum scheme; in any general- or special-purpose computer code extra measures must be built in for guaranteeing positivity of directly computed quantities and of derived quantities. The most important ones are discussed in Sec. 3.3 on monotonicity algorithms.

3. Accessory Techniques

3.1. *Formulation of Boundary Conditions*

The boundary conditions to be used with the Lagrangean scheme in solving a particular flow problem are, in principle, the same as those needed in an analytic treatment. For instance, at a left-hand boundary ξ_0, equation (57) for the jumps across the wave moving to the left and the corresponding equation (65) relating $(\partial u/\partial t)^*_0$ and $(\partial p/\partial t)^*_0$ drop out. These have to be replaced by two other equations; in a piston problem, u^*_0 and $(\partial u/\partial t)^*_0$ would be given.

Simple boundary conditions such as the reflection and the free-stream conditions may be simulated in the familiar way, namely, by adding across the boundary a slab (ξ_{-1}, ξ_0), the structure of which is a priori given or completely derived from the structure of slab (ξ_0, ξ_1).

At the origin, in cylindrical or spherical symmetry, we must have $u_{0+} = u^*_0 = (\partial u/\partial t^*)_0 \equiv 0$, while $(u/x)_{0+}$ and $(u^*/x)_{0+}$ turn into $(\partial u/\partial x)_{0+}$ and $(\partial u/\partial x)^*_{0+}$, respectively. The requirement that u_{0+} be zero implies that $\bar{\Delta}_{1/2}u$ must always be taken equal

to $2\bar{u}_{1/2}$. Since the initial derivatives with respect to ξ are assumed to be finite down to the origin, the derivatives with respect to x vanish, and Eq. (64) boils down to

$$\left\{1 - \frac{\alpha}{2(\alpha+1)}\frac{C}{W}\right\}_{0+}\left(\frac{\partial p}{\partial t}\right)_0^* = \frac{1}{2}\left\{\frac{W}{C}G\left(\frac{\partial p}{\partial e}\right)_V + \frac{1}{\alpha+1}\frac{C}{W}G^*\left(\frac{\partial p}{\partial e}\right)_V^*\right\}_{0+}. \quad (91)$$

3.2. *Eulerian Remapping*

In the present method the Eulerian equations of ICF are treated by first integrating the Lagrangean equations and then remapping the Lagrangean results onto the Euler grid (fixed or moving). This contrasts with the Euler version of Godunov's method [4], which directly integrates the Euler equations. The use of a completely separate remap step makes the method more flexible and is indispensible with regard to any multi-fluid extension. Use of a separate remap step originated with the group of W.F. Noh at Livermore, and has been applied to several codes of the Lawrence Livermore Laboratory.

The procedure of remapping is illustrated in Fig. 1. At the beginning of the Lagrangean step, the Lagrangean and Eulerian zones coincide (Fig. 1a); upon completion of the Lagrangean step they no longer do. For practical reasons we restrict the size of the time step such that no gas will cross more than one Eulerian zone boundary. In the present example the Eulerian boundaries are taken to be fixed, although in general they may be chosen to move according to some prescription.

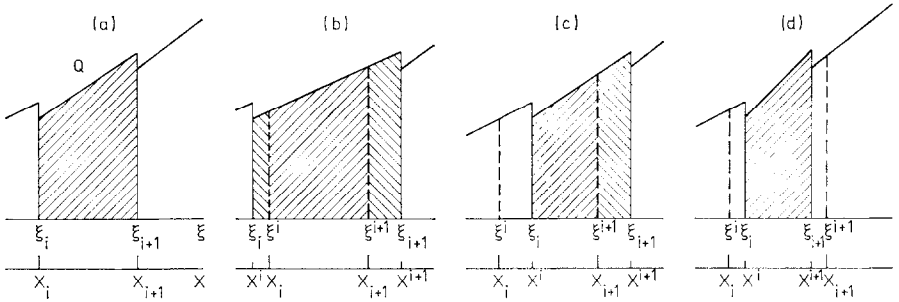

FIG. 1. Movement of a Lagrangean zone through a fixed Eulerian grid. Both mass and volume coordinates are indicated. (a) Initial coincidence of Lagrangean zone (ξ_i, ξ_{i+1}) and Eulerian zone (x_i, x_{i+1}). (b) After a Lagrangean time step the Lagrangean zone has exploded and contains the Eulerian zone. (c) The Lagrangean zone has moved to the right. (d) The Lagrangean zone has imploded and is contained in the Eulerian zone.

At the end of the Lagrangean step, an Eulerian zone may contain matter from one, two or three original Langrangean zones (Figs. 1b, 1c and 1d). In order to determine the correct structure some logic must be built into the procedure. This logic precisely is the stumbleblock in formulating ordinary finite-difference schemes that are upstream centered; see Van Leer [5].

New Lagrangean zones are now defined, coinciding again with the Eulerian zones. The new mass coordinates of the Eulerian zone boundaries are computed from the

known volume coordinates, using the updated distributions $V(t^1, \xi)$ in the original Lagrangean zones. For example, in the (most common) case of Fig. 1c, the new mass coordinate ξ^{i+1} corresponding to the fixed volume coordinate X_{i+1} may be found from the equation

$$\int_{\xi^{i+1}}^{\xi_{i+1}} \{\bar{V}^{i+1/2} + (\bar{\Delta}^{i+1/2}V/\Delta_{i+1/2}\xi)(\xi - \bar{\xi}_{i+1/2})\}\, d\xi = X^{i+1} - X_{i+1} \tag{92}$$

or

$$(\xi_{i+1} - \xi^{i+1})[\bar{V}^{i+1/2} + \tfrac{1}{2}\bar{\Delta}^{i+1/2}V\{1 - (\xi_{i+1} - \xi^{i+1})/\Delta_{i+1/2}\xi\}] = X^{i+1} - X_{i+1}\,. \tag{93}$$

The distributions of the conserved quantities resulting in the Eulerian zones in the cases of Figs. 1c and 1d are not linear in ξ. Before the next Lagrangean step can be taken these must be replaced by linear distributions. This will be done through *least-squares* fitting. A replacement distribution thus must share its zero-th moment (that is, the slab integral) and its first moment (proportional to the slope) with the replaced distribution.

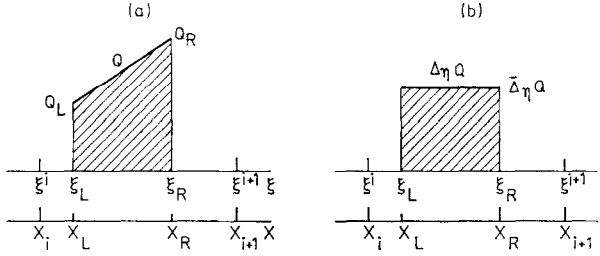

FIG. 2. A typical part of a distribution that must be remapped. It is defined in the subinterval (ξ_L, ξ_R) of (ξ^i, ξ^{i+1}), where ξ_L and/or ξ_R may of course coincide with ξ^i and/or ξ^{i+1}. Both mass and volume coordinates are indicated. (a) The distribution is linear between ξ_L and ξ_R, as for all state quantities Q. (b) The distribution is *constant* between ξ_L and ξ_R; this is true for the difference $\Delta_\eta Q$ of the state quantities in the η direction orthogonal to the sweep direction (see Sec. 3.4).

If a distribution $Q(\xi)$ is linear in the subinterval (ξ_L, ξ_R) of zone (ξ^i, ξ^{i+1}), as in Fig. 2a, the contributions from that interval to the zone integral and the first moment of Q are given by

$$\int_{\xi_L}^{\xi_R} Q\, d\xi = \tfrac{1}{2}(Q_L + Q_R)(\xi_R - \xi_L), \tag{94}$$

$$\begin{aligned}\int_{\xi_L}^{\xi_R} (\xi - \bar{\xi}^{i+1/2})\, Q\, d\xi = {} & [\tfrac{1}{2}(Q_L + Q_R) - \{(Q_R - Q_L)/(\xi_R - \xi_L)\}\{\tfrac{1}{2}(\xi_L + \xi_R) - \bar{\xi}^{i+1}\}] \\ & \times \tfrac{1}{2}\{(\xi_R - \bar{\xi}^{i+1/2})^2 - (\xi_L - \bar{\xi}^{i+1/2})^2\} \\ & + \{(Q_R - Q_L)/(\xi_R - \xi_L)\} \cdot \tfrac{1}{3}\{(\xi_R - \bar{\xi}^{i+1/2})^3 - (\xi_L - \bar{\xi}^{i+1/2})^3\}.\end{aligned} \tag{95}$$

With aid of these formulas the first two moments of any piecewise linear distribution on (ξ^i, ξ^{i+1}) can be computed. The quantity in Eq. (94) enters the slab average after division by $\Delta^{i+1/2}\xi$; the quantity in Eq. (95) enters the slope value after division by $\{(\Delta^{i+1/2}\xi)^3/12\}$. Thus, new values for $\bar{V}$ and $\bar{\Delta}V$, $\bar{u}$ and $\bar{\Delta}u$, $\bar{E}$ and $\bar{\Delta}E$ are computed for the Eulerian zones, which now are sufficiently defined to serve as the Lagrangean zones for the next time step.

The above remapping procedure involves the solution of the quadratic equation (93) for the mass $\xi_{i+1} - \xi^{i+1}$ convected across X_{i+1} in the case of Fig. 10. This costly operation may be avoided if we describe the mass distribution in the original Lagrangean zones in terms of density versus volume-coordinate rather than specific volume versus mass-coordinate. These functions $\rho(t^1, X)$ and $V(t^1, \xi)$ are related in average value by

$$\tilde{\rho}^{i+1/2} = \int_{X^i}^{X^{i+1}} \rho \, dX/\Delta^{i+1/2}X = \Delta_{i+1/2}\xi/\Delta^{i+1/2}X = 1/\bar{V}^{i+1/2}, \tag{96}$$

and in first moment by

$$\begin{aligned}
\tilde{\Delta}^{i+1/2}\rho &\equiv \int_{X^i}^{X^{i+1}} (X - \tilde{X}^{i+1/2})\, \rho(t^1, X)\, dX/\{\tfrac{1}{12}(\Delta^{i+1/2}X)^2\} \\
&= \int_{\xi_i}^{\xi_{i+1}} (X - \tilde{X}^{i+1/2})\, d(\xi - \bar{\xi}_{i+1/2})/\{\tfrac{1}{12}(\Delta^{i+1/2}X)^2\} \\
&= -\int_{X^i}^{X^{i+1}} (\xi - \bar{\xi}_{i+1/2})\, dX/\{\tfrac{1}{12}(\Delta^{i+1/2}X)^2\} \\
&= -\int_{\xi_i}^{\xi_{i+1}} (\xi - \bar{\xi}_{i+1/2})\, V(t^1, \xi)\, d\xi/\{\tfrac{1}{12}(\Delta^{i+1/2}X)^2\} \\
&\equiv -\bar{\Delta}^{i+1/2}V(\Delta_{i+1/2}\xi/\Delta^{i+1/2}X)^2 \\
&= -\bar{\Delta}^{i+1/2}V/(\bar{V}^{i+1/2})^2.
\end{aligned} \tag{97}$$

Without loss of information we may therefore exchange a linear distribution $V(\xi)$, defined by $\bar{V}$ and $\bar{\Delta}V$, for a linear distribution $\rho(X)$, defined by $\tilde{\rho}$ and $\tilde{\Delta}\rho$. Note that a tilde refers to an integration over X, just as an bar refers to an integration over ξ.

The mass convected across X_{i+1} now follows directly from

$$\begin{aligned}
\xi_{i+1} - \xi^{i+1} &= \int_{X_{i+1}}^{X^{i+1}} \{\tilde{\rho}^{i+1/2} + (\tilde{\Delta}^{i+1/2}\rho/\Delta^{i+1/2}X)(X - \tilde{X}^{i+1/2})\}\, dX \\
&= (X^{i+1} - X_{i+1})[\tilde{\rho}^{i+1/2} + \tfrac{1}{2}\tilde{\Delta}^{i+1/2}\rho\{1 - (X^{i+1} - X_{i+1})/\Delta^{i+1/2}X\}].
\end{aligned} \tag{98}$$

The density ρ is remapped with respect to X just as other quantities are remapped with respect to ξ, yielding the updated values of $\tilde{\rho}$ and $\tilde{\Delta}\rho$ in the Eulerian zones. These are

converted into $\bar{V}$ and $\bar{\Delta}V$, in preparation for the next Lagrangean step. The remapping of u and E with respect to ξ is not affected by the transformation of V into ρ.

The restriction on Δt for the composite scheme is, for each zone,

$$\Delta t \leqslant \min(\Delta x/|\bar{u}|, \Delta x/\bar{c}) + O\{(\Delta\xi)^2, \Delta\xi\,\Delta t\}; \tag{99}$$

note that this is less stringent than the usual condition for a fully Eulerian scheme:

$$\Delta t \leqslant \Delta x/(|\bar{u}| + \bar{c}) + O\{(\Delta\xi)^2, \Delta\xi\,\Delta t\}. \tag{100}$$

An additional condition is needed to prevent zone-tangling:

$$-\bar{\Delta}u\,\Delta t \leqslant \Delta x + O\{\Delta\xi(\Delta t)^2\}. \tag{100.5}$$

This need not imply a restriction of Δt, since the monotonicity algorithms of Sec. 3.3 can limit the value of $\bar{\Delta}u$ to the degree desired. Use of a monotonicity algorithm is necessary anyway, in order to prevent negative or oscillating values of zone averages.

A word remains to be said about evaluating mass coordinates. In actually programming the remap routine, ξ_i need not be given its accumulative value $\sum_{k_{\min}}^{i-1} \bar{V}_{k+1/2}^{-1}\,\Delta_{k+1/2}X$ but may be locally set equal to zero. It is not necessary to create special arrays of values of ξ_i or even $\Delta_{i+1/2}\xi$.

In the one-dimensional shock tube test of Sec. 4 the full (monotonic) remap step took about a factor 0.55 as much computing time as the full (monotonic) Lagrangean step. In the two-dimensional case the factor goes up to 0.75 because the number of state quantities that must be remapped per dimension goes up (see Sec. 3.4).

3.3. *Monotonicity Algorithms*

The monotonicity algorithms presented in the previous installment [2] for a single linear convection equation also render good service for the equations of ICF. The crudest algorithm [2, Eq. (66)] is suited for the Lagrangean scheme, while the more refined algorithm [2, Eq. (74)] is particularly useful in the Eulerian remap step.

According to [2, Eq. (66)], the onset of numerical oscillations in a monotonic sequence of slab-averages can be prevented by putting a limit to the slope of the distribution inside each slab. This limiting must be so strong that the linear distribution will not take values beyond the average values in the neighboring slabs. If the slab average is an extremum with respect to the neighboring averages, the slope must be set equal to zero. Reduction to zero is also dictated if the sign of the slope is not the same as the sign of the finite-difference slope that follows from the neighboring slab averages. The three different rules of limiting are illustrated in Fig. 3, copied from [2]. They also guarantee the preservation of positivity of the distributions.

The algebraic form of the algorithm, hence, Eq. (66) of [2], is

$$(\bar{\Delta}_{i+1/2}Q)_{\text{mono}} = \begin{cases} \min\{2\,|\,\Delta_i\bar{Q}\,|, |\,\bar{\Delta}_{i+1/2}Q\,|, 2\,|\,\Delta_{i+1}\bar{Q}\,|\}\ \operatorname{sgn}\bar{\Delta}_{i+1/2}Q \\ \qquad \text{if}\quad \operatorname{sgn}\Delta_i\bar{Q} = \operatorname{sgn}\Delta_{i+1}\bar{Q} = \operatorname{sgn}\bar{\Delta}_{i+1/2}Q, \\ 0 \qquad \text{otherwise.} \end{cases} \tag{101}$$

It must be applied to V, u and p at the beginning of the Lagrangean step.

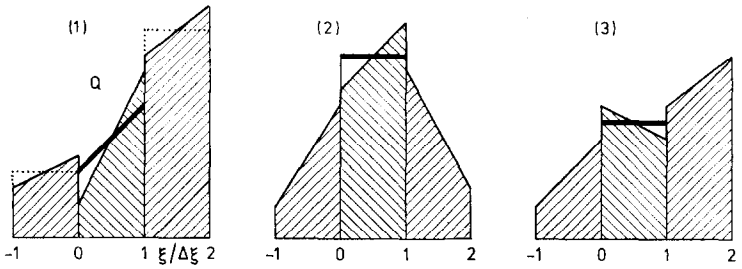

FIG. 3. The monotonicity condition (100) on the slopes at the beginning of a Lagrangean step. (1) The slope of the linear distribution (solid line) in the zone (ξ_0, ξ_1) is reduced (heavy solid line) so that the values in this zone do not go beyond the average levels (dotted line) in the adjacent zones. (2) If the mesh average reaches an extremum, the slope is reduced to zero. (3) If the slope does not agree with the trend in the mesh averages, it is also reduced to zero.

The above limiting technique will largely suppress numerical oscillations, although the nonlinearity of slab interactions makes it impossible to fully guarantee monotonicity, especially for the largest allowed time steps. In order to achieve stronger limiting the factors 2 occurring in Eq. (101) may be reduced; however, not beyond $1 + O(\Delta Q)$, lest the scheme lose its second-order accuracy. In particular, these factors may be made a decreasing function of the local Lagrangean Courant number $\sigma \equiv (\Delta t/\Delta x)\, c$, thus providing stronger limiting in regions where σ approaches unity and the numerical damping in the scheme vanishes with $1 - \sigma$. (For small Courant numbers no reduction is needed: although the numerical damping per time step vanishes with σ, damping per unit time does not). Note that any oscillations still created in the Lagrangean step will be partly damped through the limiting in the Eulerian remap step.

If the factors 2 are replaced by 0, the slopes will always be set equal to zero and the Lagrangean scheme reduces to Godunov's scheme. This may be a convenient option

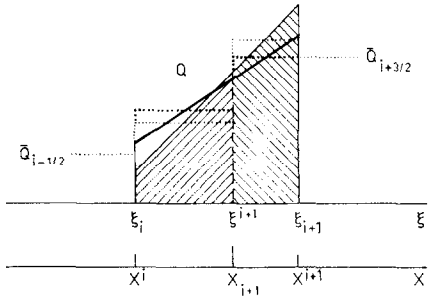

FIG. 4. The monotonicity condition (102) on the slopes at the beginning of an Eulerian remap step. Both mass and volume coordinates are indicated. The slope of the linear distribution (solid line) in the Lagrangean zone (ξ_i, ξ_{i+1}) is reduced such that the average value (dotted line) in the part of the zone that has crossed/not crossed the Eulerian zone boundary X_{i+1} does not overshoot/undershoot the average value in the adjacent Lagrangean zone (dotted line). The adjusted distribution and corresponding average levels in the zone parts are indicated by heavy solid and heavy dotted lines, respectively.

to have in a computer program, when comparisons with a first-order method have to be made.

The algorithm [2, Eq. (74)] does allow the values of a state quantity inside some slab to go beyond the range spanned by the neighboring-slab averages. But the average value in the part of the slab that, in the next convection step, will cross a zone boundary, as well as the average value in the part that will stay behind, must remain within that range. This condition can be met, again, by limiting the slope of the distribution of the quantity, as shown in Fig. 4. Note that positivity is guaranteed only for the zone *averages*.

Obviously, this milder kind of limiting is applied most easily if the amount of material to be convected across the zone boundaries is known beforehand, as in the case of a constant convection speed [2]. Fortunately, this condition is met, too, in the Eulerian remap step. The limiting formula for the case of Fig. 4 is identical to [2, Eq. (74)] and reads

$$(\bar{\Delta}^{i+1/2}Q)_{\text{mono}} = \begin{cases} \min\left\{\dfrac{2}{\varphi_{i+1}} \mid \Delta^i\bar{Q} \mid, \mid \bar{\Delta}^{i+1/2}Q \mid, \dfrac{2}{1-\varphi_{i+1}} \mid \Delta^{i+1}\bar{Q} \mid\right\} \operatorname{sgn} \bar{\Delta}^{i+1/2}Q \\ \quad \text{if} \quad \operatorname{sgn} \Delta^i\bar{Q} = \operatorname{sgn} \Delta^{i+1}\bar{Q} = \operatorname{sgn} \bar{\Delta}^{i+1/2}Q, \\ 0 \quad \text{otherwise,} \end{cases} \tag{102}$$

where

$$\varphi_{i+1} = (\xi_{i+1} - \xi^{i+1})/\Delta_{i+1/2}\xi \tag{103}$$

is the mass fraction of the Lagrangean slab (ξ_i, ξ_{i+1}) that has crossed the Eulerian zone boundary x_{i+1}. The algorithm must be used after the new mass coordinates of the Eulerian zone boundaries have been obtained but before the new Eulerian slab averages are computed.

A complication would arise if we use Eq. (102) to adjust $\bar{\Delta}^{i+1/2}V$. Changing this quantity means changing the mass distribution in the convected Lagrangean zone and, therefore, changing the mass fraction of the zone that has crossed an Eulerian boundary. The mass fraction, however, feeds back into the monotonicity algorithm (102). This complication disappears if, as advised in Sec. 3.2, we redistribute the density over the volume coordinate, rather than the specific volume over the mass coordinate.

In the case of Fig. 4, the monotonicity condition for $\tilde{\Delta}^{i+1/2}\rho$ namely does not involve the mass fraction φ_{i+1} but the volume fraction $f_{i+1} \equiv (X^{i+1} - X_{i+1})/\Delta^{i+1/2}X$, which is already known and will not be affected by a change in $\rho(X)$. We may directly apply the algorithm (102), with φ replaced by f and overhead bars by tildes, to $\tilde{\Delta}^{i+1/2}\rho$, whereupon φ_{i+1} is determined with aid of Eq. (98). Then the application of (102) to $\bar{\Delta}^{i+1/2}u$ and $\bar{\Delta}^{i+1/2}E$ follows as usual.

As mentioned in [2], monotonicity algorithms like (101) and (102) will clip real peaks to the same degree as a first-order method would do. This happens in particular for V, p and E at reflecting boundaries, where these quantities always have an extremum. The algorithms may be improved by including extra information on what the distributions looked like prior to their replacement by linear distributions.

For example, consider a purely Lagrangean calculation. At the end of each step we know the interface values of V, u and p, as computed in Eqs. (85)-(87). We may save

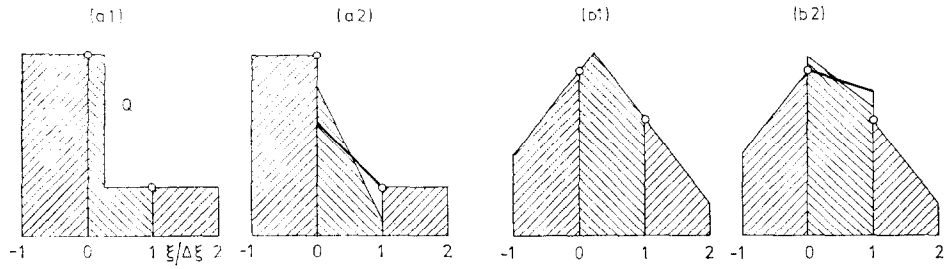

FIG. 5. The monotonicity condition (104) on the slopes in a purely Lagrangean calculation. (a1) The actual initial values represent a shock inside slab (ξ_0, ξ_1). (a2) The shock structure is replaced by a linear distribution, which subsequently is monotonized (heavy line). The condition is that the distribution inside (ξ_0, ξ_1) must not take values outside the range indicated by the actual interface values at ξ_0 and ξ_1 (tack marks). Since those values are the same as the average values in the adjacent slabs, we might as well have used condition (101). Note that the slope determined by interface differencing is the same regardless how far the shock has advanced in the zone. After monotonization, however, the slope does respond to the shock advancement. (b1) The actual initial values have a peak inside slab (ξ_0, ξ_1). (b2) The peaked distribution is replaced by a linear one, which subsequently is monotonized (heavy line). The highest value allowed to appear in the slabs is the original interface value at ξ_0. According to condition (101) the distribution would have become flat and the slope in slab (ξ_{-1}, ξ_0) would be slightly reduced.

these values rather than just save their differences, computed in Eqs. (88)-(90). We first apply the limiter (101), keeping track of where it actually limits $\bar{\Delta}Q$. Only in those places we also try out the narrow-base limiter

$$(\bar{\Delta}^{i+1/2}Q)_{\text{mono}} = \begin{cases} \min\{2 \mid Q^{i+1} - \bar{Q}^{i+1/2} \mid, \mid Q^{i+1} - Q^i \mid, \\ \qquad 2 \mid \bar{Q}^{i+1/2} - Q^i \mid\} \operatorname{sgn}(Q^{i+1} - Q^i) \\ \qquad \text{if } \operatorname{sgn}(Q^{i+1} - \bar{Q}^{i+1/2}) = \operatorname{sgn}(\bar{Q}^{i+1/2} - Q^i) = \operatorname{sgn}(Q^{i+1} - Q^i), \\ 0 \qquad \text{otherwise,} \end{cases} \tag{104}$$

which will yield the same limiting as (101) near a plateau but weaker limiting near a peak; see Fig. 5. If indeed (104) yields the weaker limiting, the value of $\bar{\Delta}Q$ given by (104) is adopted.

While slope limiting is a powerful tool in achieving monotonicity or positivity, there are circumstances when additional measures must be taken. For instance, the internal energy $\bar{e}$ in a slab may become negative as a consequence of its smallness with respect to the total energy $\bar{E}$ or to a negative source term $\langle \bar{G} \rangle \Delta t$. Such errors can always be avoided, although not most efficiently, by reducing the time step. If the danger of negativity is limited to a few zones, the time step need only be reduced locally, requiring multiple time steps in the danger area. A discussion of such techniques, which are not specific for MUSCL, falls outside the scope of this paper.

3.4. *Time Splitting*

The multi-dimensional Eulerian flow equations, formulated on the basis of an orthogonal coordinate system, may be approximated with second-order accuracy by

applying the one-dimensional Eulerian scheme in alternating directions according to the well-known time-splitting algorithm of Strang [6]. The method of time-splitting has become popular in fluid dynamics mainly because it makes our knowledge of one-dimensional schemes directly applicable to the multi-dimensional case. The decomposition of a multi-dimensional numerical operator into one-dimensional components, however practical, makes it difficult to satisfy intrinsically multi-dimensional conservation rules, e.g., irrotationality. Particularly in incompressible flow the results of time-splitting are not always satisfactory; see e.g. Fromm [20]. A discussion of the pros and cons of time-splitting seems not appropriate here.

The number of independent state quantities to be integrated by the n-dimensional second-order method is $(n + 1)(n + 2)$, of which $n + 2$ are the slab averages of V, E and n velocity components, and $n(n + 2)$ are the first moments of each of the $n + 2$ state quantities in n directions. When doing a sweep in one direction, the velocities and the derivatives in the other directions play no role in computing the interaction of slabs. In the Lagrangean step they remain unaffected while in the Eulerian remap step their distributions along the sweep axis are remapped as usual.

For example, suppose that there is a second dimension with space coordinate y, volume coordinate Y, mass coordinate η and velocity v. In each Eulerian zone are given $\bar{v}$, $\bar{\Delta}_\xi v$ and $\bar{\Delta}_\eta v$. When doing a Lagrangean step in the x-direction, these values do not change; when remapping, the piecewise linear distribution of v over ξ yields new values of $\bar{v}$ and $\bar{\Delta}_\xi v$ in an Eulerian zone just as in the example of Sec. 3.2. (see Fig. 2a). The piecewise *constant* distribution of $\bar{\Delta}_\eta v$ over ξ is averaged to yield the new value of $\bar{\Delta}_\eta v$ in an Eulerian zone (see Fig. 2b).

For the mass coordinate ξ_i in the x-direction of some Eulerian zone stretching from y_j to y_{j+1} in the y-direction, the mass accumulated between y_j and y_{j+1} up to x_i may be taken. The mass coordinates η_j are defined similarly. When sweeping in one direction, the mass coordinates in the orthogonal direction are affected. They need not be remapped as the other quantities, but may be reconstructed during the next sweep in the orthogonal direction. See, however, the remark concluding Sec. 3.2.

Multi-dimensional boundary conditions that must be applied to surfaces not orthogonal to any of the coordinate axes may be decomposed into a sequence of one-dimensional orthogonal boundary conditions just as done in the SLIC method (Simple Lagrangean Interface Calculation) of Noh and Woodward [7] for the boundaries between different fluids. A refinement of that method has recently been formulated by Woodward [8], with particular reference to the physics of slab interaction included in the present second-order scheme.

4. Numerical Examples

To illustrate the performance of the method described previously, some one- and two-dimensional results obtained with the MUSCL code are shown in Figs. 6-11.

Fig. 6 shows the results of an application of the method to the same one-dimensional shock tube problem as Sod [18] used for testing twelve schemes and combina-

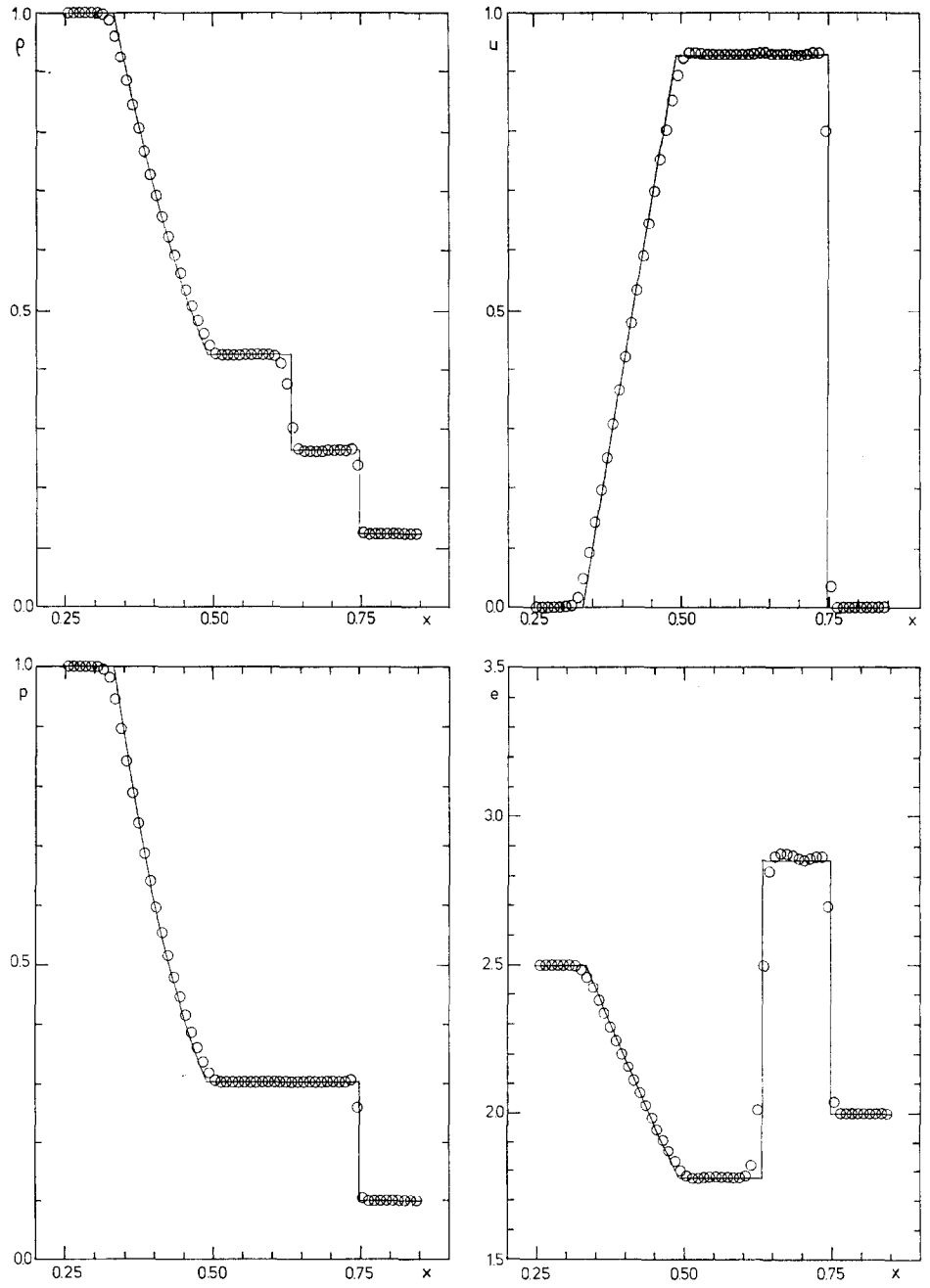

FIG. 6. Exact solution (line) and cell averages (circles) of ρ, u, p and e obtained with MUSCL (Eulerian) for the same exploding diaphragm problem as used by Sod [18]. Initial values: $u \equiv 0$; $\rho = p = 1$ for $x < 0.5$; $\rho = 0.125$, $p = 0.1$ for $x > 0.5$; $\gamma = 1.4$. Courant number 0.9; $\Delta x = 0.01$. Output after 34 time steps at $t = 0.14154$.

tions of schemes. The tube extends from $x = 0$ to $x = 1$ and is divided in 100 computational cells. The gas is initially at rest, while at $x = 0.5$ the density and the pressure jump down a factor 8 and a factor 10, respectively. Numerical and exact solutions for ρ, u, p and e are displayed at the time that the shockwave moving to the right has approximately reached $x = 0.75$. The figure allows direct comparison with Sod's figures and indicates that the present method is superior to all methods tested by Sod, including Phoenical SHASTA [3]. The latter scheme, however, was used with too high a value of the Courant number, so that monotonicity was not preserved.

For this 100-cell one-dimensional flow problem the CPU time required for advancing one time step with MUSCL on the IBM 370/158 of Leiden University (MVS operating system) was 0.47 seconds, corresponding to 0.17 seconds on the CDC 6600 (SCOPE 3.4 operating system) of the Energy Center of the Netherlands in Petten. These numbers do not include calls to plotting routines and therefore can not directly be compared to the running times given by Sod, which are substantially larger. Furthermore, Sod's coding of the various schemes may not have been optimized.

Figs. 7, 8, 9 and 10 show some two-dimensional results obtained with MUSCL by P. Woodward at Leiden Observatory. Drawn are pressure contours for flow at Mach 3 through a tunnel with a step, in the case of plane symmetry. At $t = 0$ the flow is impulsively started everywhere in the tunnel; across the left-hand boundary inflow at Mach 3 persists ($u_{-\infty} = 3$, $c_{-\infty} = 1$), while across the right-hand boundary free outflow is prescribed. The height of the step is one fifth the entrance height H of the tunnel, while the length of the narrow part of the tunnel is 2.4 times the entrance width.

The pictures 7-9 show the flow after about 4 vertical sound-crossing times $H/c_{-\infty}$ for grids with different mesh sizes. In all cases the meshes are square and the timestep used was 90 % of the maximum allowed by condition (99). Fig. 7 gives the most detail, with H covered by 20 meshes, while in Fig. 8 H is covered by 10 meshes.

Fig. 9 shows what MUSCL achieves when the tunnel entrance is only 5 meshes high and the step, therefore, only one mesh. The Mach stem still appears to be visible; however, it is an artifact due to the monotonicity algorithms (101) and (102) which force pressure contours to be perpendicular to a reflecting wall (see the conclusion of Sec. 3.3). The performance on a grid this coarse could be substantially improved through the use of the narrow-base monotonicity criterion (104).

The results in Figs. 7-9 are far from stationary. The steady flow pattern, obtained after 16 vertical sound-crossing times with a grid of 45×15 meshes, is shown in Fig. 10.

The remaining Fig. 11 shows the results of Godunov's method, approximately realized in MUSCL by setting all slopes equal to zero through an over-restrictive monotonicity condition (see Sec. 3.3). These results for $H/\Delta y = 30$ are mimicked by the second-order MUSCL scheme with $H/\Delta y = 10$ (Fig. 8). This means a dramatic increase in efficiency when going to second order, since Godunov's method, even when programmed efficiently, will not run more than twice as fast as MUSCL.

The execution speed of MUSCL appears to be quite satisfactory. For the 1008-cell grid of Fig. 7, a time step on the IBM 370/158 with MUSCL requires 8.78 seconds,

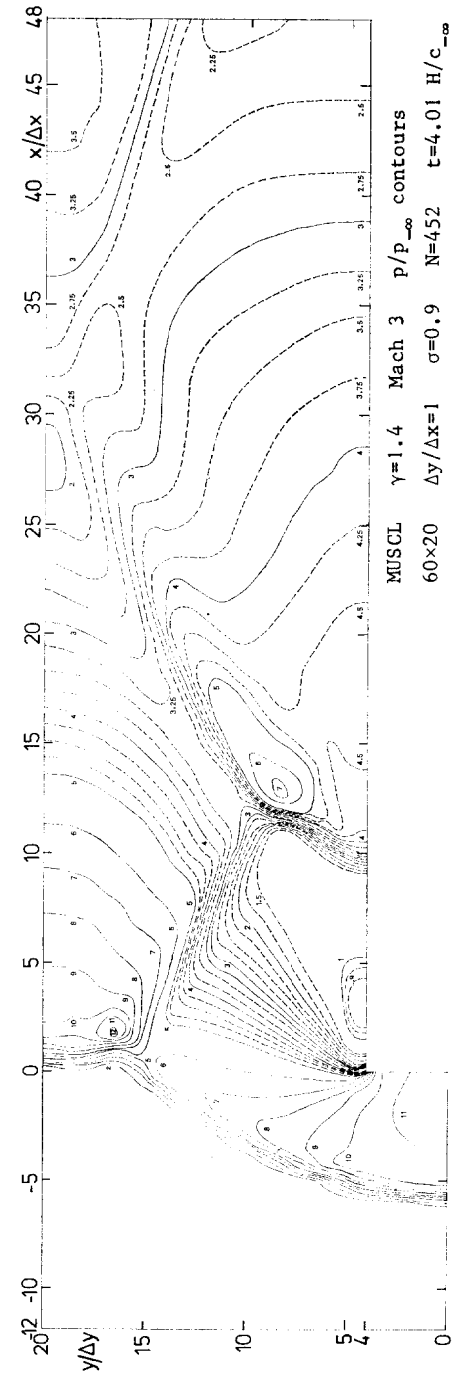

FIG. 7. Pressure contours at $t = 4H/c_{-\infty}$, obtained with the second-order MUSCL code, for Mach 3 flow in a windtunnel with a step (plane symmetry). Entrance height 20 zones, step height 4 zones. Sonic/convective Courant condition (99) used with safety factor 0.9. The contours are drawn using the information contained in the average values *and* the slopes given for each Eulerian zone. Courtesy of P. R. Woodward.

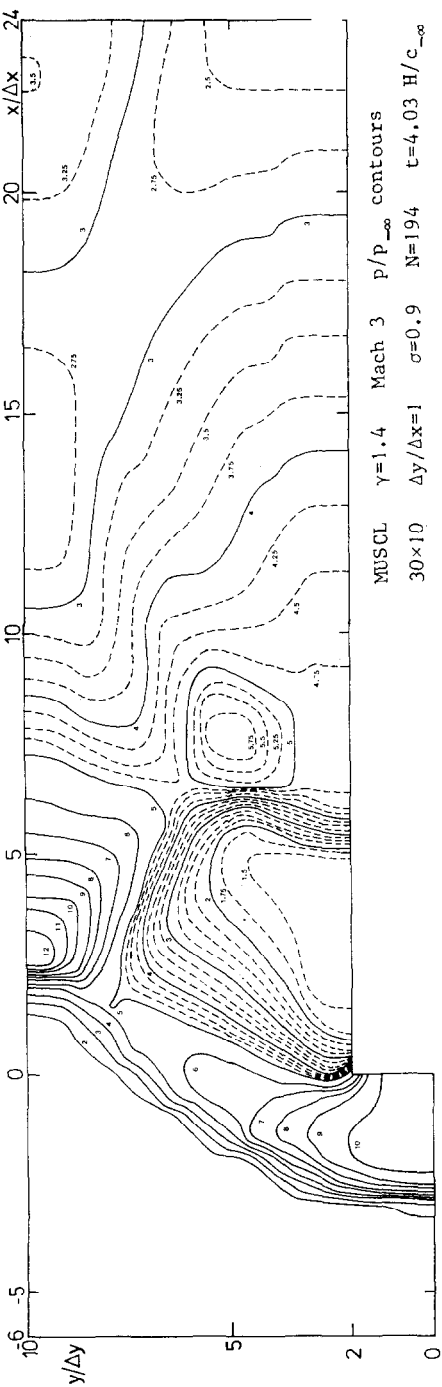

FIG. 8. Same as Figure 7, but for an entrance height of 10 zones and a step height of 2 zones.

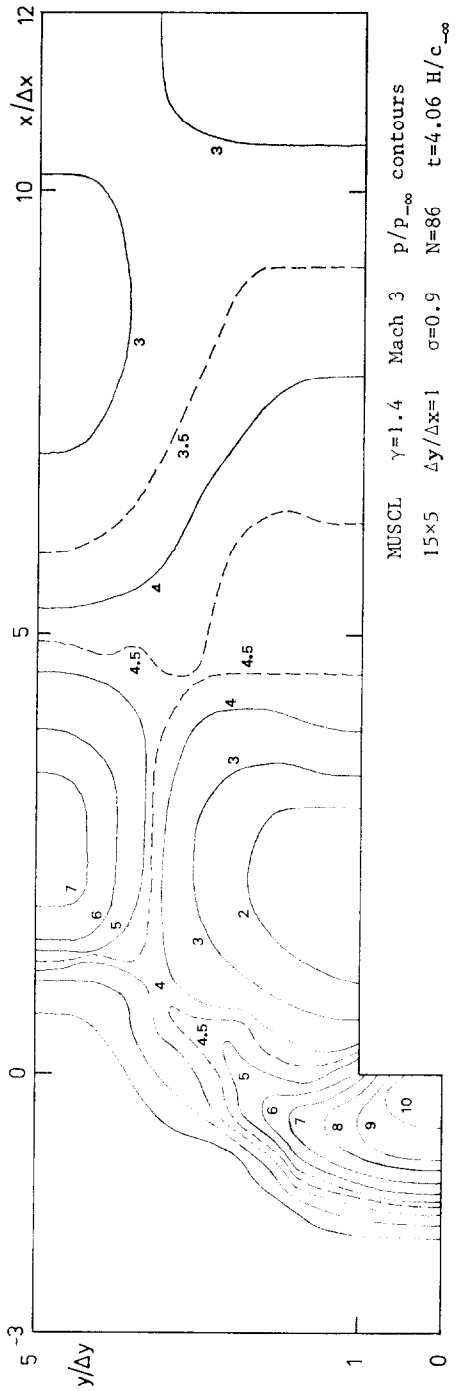

FIG. 9. Same as Figure 7, but for an entrance height of 5 zones and a step height of 1 zone.

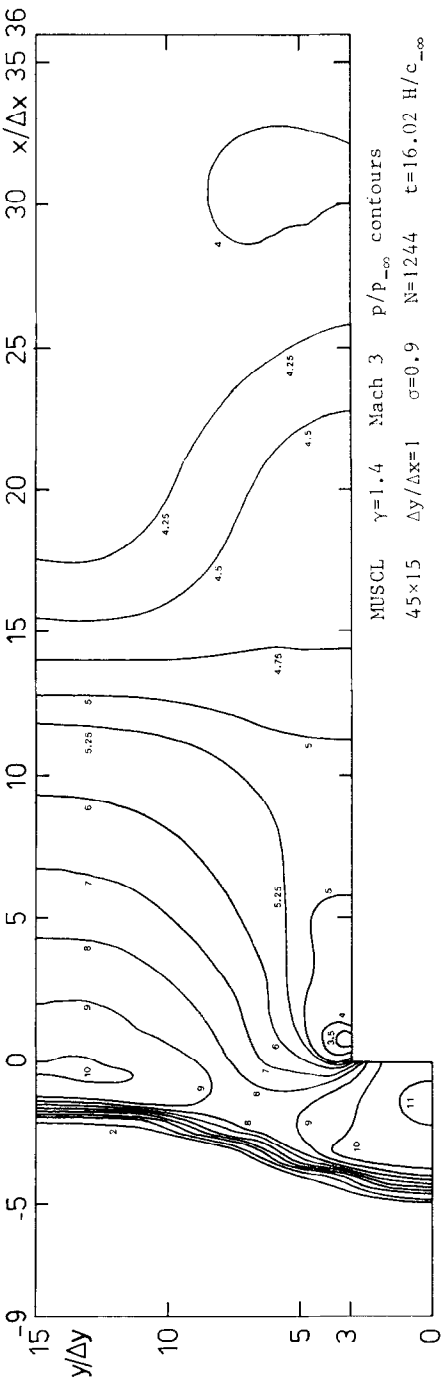

FIG. 10. Same as Figure 7, but at $t = 16\ H/c_{-\infty}$, for an entrance height of 15 zones and a step height of 3 zones.

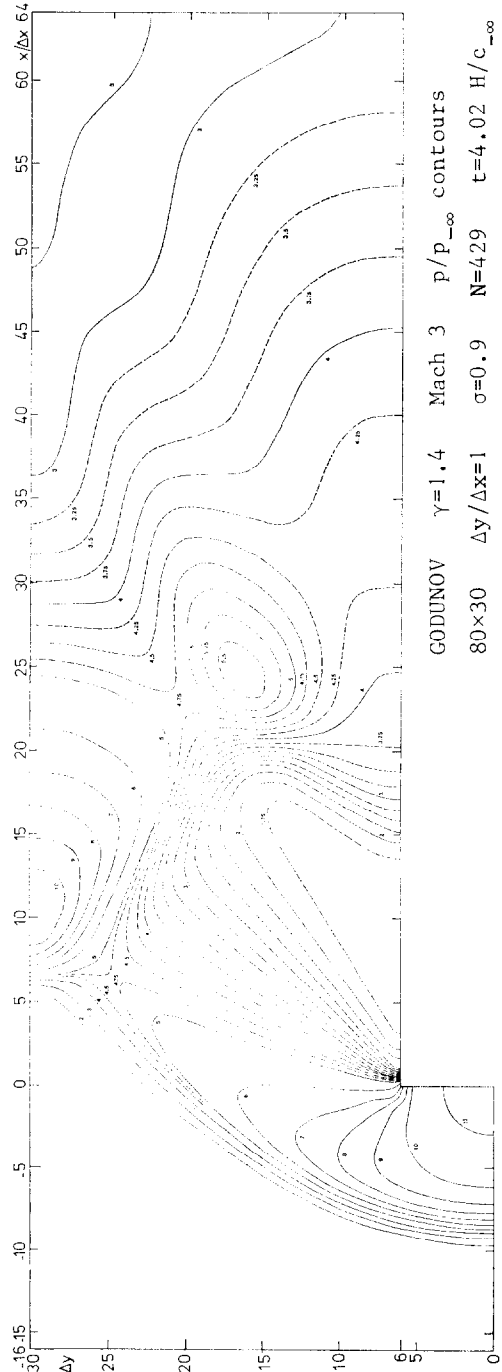

FIG. 11. Same as Figure 7, but obtained with Godunov's scheme, realized approximately in the MUSCL code by "monotonizing" all slopes down to zero. Entrance height 30 meshes, step height 6 meshes.

or 2.33 times as much as the ALFVEN code [9], developed by W. J. Weber of Utrecht Observatory on the basis of Phoenical SHASTA [3]. The latter code, however, must run at values of the sonic and convective Courant numbers not greater than one half, so that MUSCL ends up being 15-20 % slower than ALFVEN in absolute time advancement. The difference of a factor 2 to 3 in CPU time between a MUSCL step and an ALFVEN step is readily explained by the fact that in a two-dimensional calculation, with the MUSCL code three times as many independent state quantities are updated as with the ALFVEN code. The above lambda-shock problem has not yet been run satisfactorily with ALFVEN, but a linear error analysis and the comparative shock-tube test give no reason to believe that ALFVEN would be more accurate than MUSCL.

Recently, Boris and Book formulated a low-phase-error SHASTA-like algorithm, explicit FCT-LPE [10], that may be more accurate and efficient than the present version of MUSCL. As mentioned earlier, in MUSCL there is room for improvement, too. Provisional results obtained by Woodward [16], using least-squares fitting of slopes and the slope limiter (104) in the Lagrangean step, show a dramatic increase in accuracy for coarse grids. A comparison between the latest version of MUSCL and other codes has been projected.

In conclusion, the present method for ICF appears to be at least as efficient as other good second-order methods. Those already addicted to Godunov's first-order method may welcome the second-order method as an extension with greatly increased efficiency.

5. Conclusions and Desiderata

The integration scheme for the equations of ideal compressible flow presented in this fifth installment of the series "Towards the Ultimate Conservative Difference Scheme" combines the ideas developed in the foregoing instalments.

The goal of the work reported in the series was to derive a second-order method for ICF not plagued by the pests arising in the use of Lax-Wendroff type schemes, that is, oscillatory solutions, nonlinear instabilities and large, predominantly negative, phase errors. That such a method might very well exist was indicated by Fromm [11], whose "zero-average phase error" scheme for the convection of vorticity actually is the simplest upstream-centered second-order convection scheme. Fromm's scheme was regarded by me as a good candidate for conversion into a conservative scheme for ICF. But first the matter of numerical oscillations had to be settled.

In the first installment [12] the basic technique for preserving monotonicity during one-dimensional convection was developed on the basis of the Lax-Wendroff scheme. When made monotonic, the latter scheme loses the conservation form: it involves too few (three) initial values to combine monotonicity and conservation. Fromm's scheme, based on four initial values in an upstream-centered sequence of nodal points, offers the freedom to achieve this desirable combination. This was shown in the second installment [13]. As explained in the third installment [5], the conversion of

Fromm's convection scheme into a scheme for ICF offers serious problems, in particular because of the upstream centering.

The solution to these problems was to follow Godunov's [1] way of turning the first-order upstream convection scheme (used before by Courant, Isaacson and Rees [14] for the characteristic equations of ICF) into a conservative scheme for ICF. Godunov uses the control-volume formulation to ensure conservation and therefore works with slab-averaged values of state quantities, rather than with nodal-point values. When reformulating Fromm's convection scheme for a control volume it turned out that the scheme could be greatly improved if, in addition to the slab averages, independent slab-averaged gradient values are used to represent the distribution of the convected quantity. The monotonicity algorithm derived in [5] boils down to a prescription for limiting these gradients. This was reported in the fourth installment [2].

In the present installment, the upstream-centered convection schemes from [2] are forged into the method in two places. In the Lagrangean step, the interaction of gas slabs at their interface is calculated by inserting upstream-centered information into the characteristic equations. This has the effect of convecting the Riemann invariants $J^{\pm}$ along the characteristics $I^{\pm}$ with an upstream-centered scheme. Furthermore, in the Eulerian remap step, Eulerian results are obtained from the Lagrangean results by convecting the Lagrangean distribution through the Eulerian grid with aid of another upstream-centered scheme. Note that the latter approach differs from Godunov's [4], where the Eulerian equations are approximated in a single step with an upstream-centered scheme.

The various monotonicity algorithms from [2] also find their place in both the Lagrangean and the Eulerian step.

Having been climbing up, five installments long, towards the ultimate conservative scheme (which must be regarded as a symbol of man's never-ending striving for perfection rather than one particular method waiting for its discovery), I feel like having reached a plateau wide enough to allow a good stretch. The plateau may be widened by removing some already loose rocks: barriers that stand in the way of improvement of the accuracy and the efficiency of the method. Some desirable improvements are the implementation of least-squares fitting of the distributions at the end of the Lagrangean step, of a monotonicity algorithm that clips peaks less strongly, and of approximate adiabats in the calculation of slab interactions, useful for an arbitrary equation of state.

The surroundings of the plateau invite some interesting small excursions, for instance, to the domain of shallow-water flow. The lowest order shallow-water equations have the same form as those used presently, with $p \sim V^{-2}$ and the energy equation missing, and are easily incorporated in the method.

A major excursion would be the implementation of the method for ideal compressible magneto-hydrodynamics. This would require a full reconsideration of the slab interaction problem and a rederivation of the associated formulas. It is the price we have to pay for including in the method more of the physical content of the underlying equations than just their conservation form.

APPENDIX A: NUMERICAL RESOLUTION OF A FLOW DISCONTINUITY

How to resolve an arbitrary flow discontinuity is illustrated in Figures A1, A2 and A3, which are diagrams of pressure versus velocity. In Figure A1 are indicated the initial states $I_- = (u_-, p_-)$ and $I_+ = (u_+, p_+)$ and the two curves $\mathscr{A}_-$ and $\mathscr{A}_+$ representing all states that can be reached from I_- and I_+ through a rarefaction wave or a shock wave. The waves generating $\mathscr{A}_-$ move to the left, those generating $\mathscr{A}_+$ move to the right. The rarefaction branch (Poisson adiabat) and the shock branch (Hugoniot curve or shock adiabat) of such curves have different equations, corresponding to the different expressions (34γ) and (31γ) for the wave speeds. As follows from Eq. (25), the wave speeds $-W_-$ and W_+ appear in the diagram as the slopes of the chords drawn from I_- and I_+ to the points representing the respective post-wave states. In the weak-wave limit, these chords become the tangents to $\mathscr{A}_-$ and $\mathscr{A}_+$ at I_+ and I_-; the absolute values of their slopes are the initial sound speeds C_- and C_+. The intersection point of the curves represents the resolved state $R = (u^*, p^*)$. In Figure A1 this state results from a rarefaction wave facing left and a shock wave facing right. For an extensive discussion of such diagrams see e.g. Courant and Friedrichs [15].

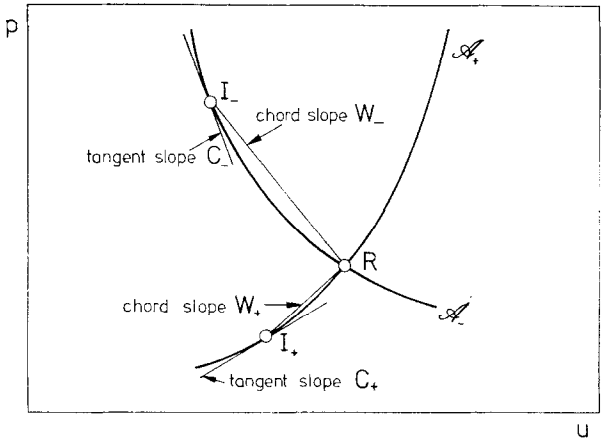

FIG. A1. Resolution of an flow discontinuity, as represented in the (u, p) plane. The resolution involves a rarefaction wave moving to the left and a shock wave moving to the right.

The equations of the adiabats are too complicated to allow explicit evaluation of u^* and p^*. The iterative procedure for finding R indicated by Godunov [1] is illustrated in Figure A2, for the case of two shock waves. As a first guess for p^* we may adopt the pressure value from the state $R^{(1)} = (u^{*(1)}, p^{*(1)})$ that is found by intersecting the tangents to $\mathscr{A}_-$ and $\mathscr{A}_+$ at I_- and I_+. Algebraicly it is given by Eq. (60).

Next, $p^{*(1)}$ is inserted into the appropriate formula (either (34γ) or (31γ)) to yield $W_-^{(1)}$ and $W_+^{(1)}$. In the picture this is indicated by drawing the chords from I_- and I_+ to the points $R_-^{(1)}$ and $R_+^{(1)}$ on $\mathscr{A}_-$ and $\mathscr{A}_+$ where the pressure equals $p^{*(1)}$; the associated

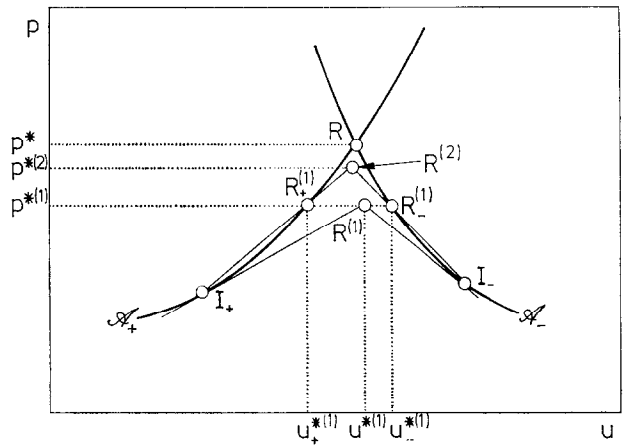

FIG. A2. Godunov's iterative method of resolving a flow discontinuity, illustrated in the (u, p) plane. Double shock case.

velocities are called $u_-^{*(1)}$ and $u_+^{*(1)}$. Intersecting those chords yields the second estimate $p^{*(2)}$, the algebraic value of which is found by inserting $W_-^{(1)}$ and $W_+^{(1)}$ into Eq. (59). The iterations are continued till the desired accuracy is reached; then u^* follows from inserting the latest wave-speed value into Eq. (61).

Godunov's procedure reduces the difference between the iterated and exact pressure values by a factor $O\{(u_+ - u_-), (p_+ - p_-)\}$ per iteration cycle. P. J. Bedijn of Leiden Observatory suggested a more efficient procedure, advancing a factor $O\{(u_+ - u_-)^2, (p_+ - p_-)^2\}$ in accuracy per iteration cycle; this is illustrated in Figure A3 for the case of two rarefaction waves. Instead of intersecting chords drawn from $I_\pm$ to $R_\pm^{(n)}$ to

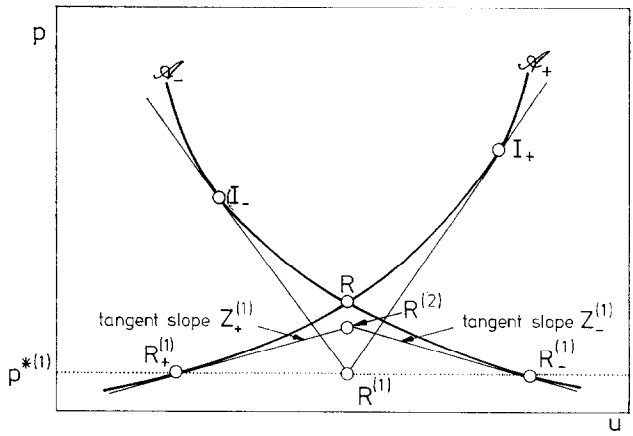

FIG. A3. A second-order iteration method of resolving a flow discontinuity, illustrated in the (u, p) plane. Double rarefaction case.

arrive at $R^{(n+1)}$, we intersect the *tangents* to $\mathscr{A}_\pm$ in the points $R^{(n)}$. The equation for $p^{*(n+1)}$ becomes

$$p^{*(n+1)} = p^{*(n)} - Z_-^{(n)} Z_+^{(n)} (u_+^{*(n)} - u_-^{*(n)})/(Z_-^{(n)} + Z_+^{(n)}), \tag{A1}$$

where $Z_-^{(n)}$ and $Z_+^{(n)}$ are the absolute values of the tangent slopes. The faster convergence is achieved at a minor extra expense of computing time. The tangent slope value namely is a byproduct of the wave speed calculation; on a curve $\mathscr{A}$ through the initial state (u, p) we have

$$\left| \frac{dp^*}{du^*} \right|_{\mathscr{A}} = \begin{cases} \dfrac{2W^2}{W^2 + C^2} W & \text{if } p^* \geqslant p, \\ C^* = C(p^*/p)^{1-(\gamma-1)/(2\gamma)} & \text{if } p^* < p. \end{cases} \tag{A2γ}$$

When calculating the wave speeds $W_\pm^{(n)}$, which are needed to obtain $u_\pm^{*(n)}$ from Eqs. (58) and (57), the tangent slopes $Z_\pm^{(n)}$ can be evaluated from the intermediate results; in particular, no extra square root or exponentiation is involved. Once p^* has been obtained with sufficient accuracy, u^* follows from the latest values of $u_\pm^*$ and $Z_\pm$ through

$$u^* = (Z_- u_-^* + Z_+ u_+^*)/(Z_- + Z_+). \tag{A3}$$

A pressure value resulting from the intersection of chords or tangents, in particular $p^{*(1)}$, may become negative if $u_+ \gg u_-$. The pressure value must therefore be limited downward by the smallest value $p_{\min}$ that is significant for the flow considered. If and only if $p^{*(2)}$ is negative again, the exact solution would involve cavitation and p^* can be left at $p_{\min}$ (see Fig. A4). For u^* we may take $u^{*(2)}$.

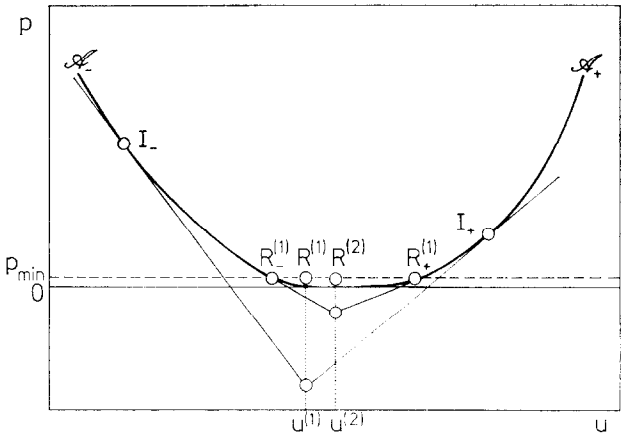

FIG. A4. Failure of the second-order resolution method in case the flow cavitates.

APPENDIX B: UPDATING SLOPES

In the previous paper [2] of the present series, three ways of updating a slope were presented, namely, conventional finite differencing, interface differencing and least-squares fitting. Following the first way, a slope value is obtained by centrally differencing the average values in the adjacent slabs; in a uniform grid we have

$$\bar{\Delta}_{i+1/2}Q = \tfrac{1}{2}(\Delta_i\bar{Q} + \Delta_{i+1}\bar{Q}) = \tfrac{1}{2}(\bar{Q}_{i+3/2} - \bar{Q}_{i-1/2}). \tag{B1}$$

Such a value need not be stored along with the slab averages.

The second way, differencing interface values, has been followed in the Lagrangean step (Secs. 2.2, 2.4) while the third way, basing the slope value on the first moment of the distribution, has been followed in the Eulerian remap step. Both techniques require separate storage of the slope value.

A linear analysis of the present method, given in [2], shows that the moment-fitting technique of Section 3.1 (represented by scheme III in [2]) is vastly superior to the other finite-difference techniques: its evolutionary convective error is the smallest by two orders of $\Delta\xi$. Interface-value differencing (scheme II) and slab-average differencing (scheme I) have equal convection errors (for $\Delta t/\Delta\xi \to 0$), whereas the maximum dissipative error per time step in the former is a factor 3 smaller than in the latter, but still a factor 3 larger than for moment-fitting.

A peculiarity of interface-value differencing is that it can drastically change the slope value over a vanishingly small time step. For example, a shock wave barely penetrating into a uniform slab will raise all slope values in that slab from zero to the jump values divided by $\Delta\xi$. The effect can be offset by application of a monotonicity algorithm, which is recommended anyway (see Fig. 5a).

Slab-average differencing has the inherent disadvantage of involving data from neighbouring slabs. This, of course, is the cause of its larger dissipation error; it also leads to extra errors if the difference is taken across a strong contact discontinuity or a point where the mesh is suddenly refined a factor $O(1)$. These extra errors also occur in Godunov's method [1, Sec 7]. The main advantage of differencing slab averages is a reduction in computer storage space, as compared to the requirements of the other ways of evaluating a slope.

With slab-average differencing, the scheme for convecting the Riemann invariants, underlying the present method, boils down to the upstream-centered second-order scheme of Fromm [12], just as Godunov's method boils down to the upstream-centered first-order scheme of Courant, Isaacson and Rees [15].

For those who appreciate the simplicity of determining slopes by slab-average differencing, it is useful to know there is a way of doing this so that the crudest monotonicity condition is automatically accounted for. As indicated in [2, Eq. (67)], in a uniform grid one simply has to determine $\bar{\Delta}_{i+1/2}Q$ by *harmonically* averaging $\Delta_i\bar{Q}$ and $\Delta_{i+1}\bar{Q}$, rather than algebraically:

$$(\bar{\Delta}_{i+1/2}Q)_{\text{mono}} = \begin{cases} \dfrac{2\,\Delta_i\bar{Q}\,\Delta_{i+1}\bar{Q}}{\Delta_i\bar{Q} + \Delta_{i+1}\bar{Q}} & \text{if} \quad \operatorname{sgn}\Delta_i Q = \operatorname{sgn}\Delta_{i+1}\bar{Q}, \\ 0 & \text{otherwise.} \end{cases} \tag{B2}$$

In the Eularian remap there is no excuse for not using the least-squares formula. In the Lagrangean step, however, least-squares fitting offers serious problems. To illustrate these, let us multiply Eq. (1) by $(\xi - \bar{\xi})$ and integrate it over one Lagrangean zone and one time step; this leads to a formula for updating $\bar{\Delta}V$:

$$\tfrac{1}{12}(\Delta_{i+1/2}\xi)^2(\bar{\Delta}^{i+1/2}V - \bar{\Delta}_{i+1/2}V) + \Delta_{i+1/2}\xi(\bar{X}^{i+1/2} - \bar{X}_{i+1/2}) - \tfrac{1}{2}\Delta t\,\Delta_{i+1/2}\xi(\langle x^\alpha u\rangle_i + \langle x^\alpha u\rangle_{i+1}) = 0, \tag{B3}$$

or

$$\bar{\Delta}^{i+1/2}V = \bar{\Delta}_{i+1/2}V + 6(\Delta t/\Delta_{i+1/2}\xi)[\langle x^\alpha u\rangle_i + \langle x^\alpha u\rangle_{i+1} - 2\langle\overline{x^\alpha u}\rangle_{i+1/2}] = 0. \tag{B4}$$

The term between square brackets is of the order $O\{(\Delta\xi)^2\}$ and can not be calculated adequately without knowledge of the *second* time derivative of u at the interfaces. If we leave an error

$$\tfrac{1}{6}(\Delta t)^2\{\partial^2(x^\alpha u)/\partial t^2\}_{i,i+1}$$

in $\langle x^\alpha u\rangle_{i,i+1}$, as in Eq. (69), but, likewise, an error

$$\tfrac{1}{6}(\Delta t)^2\{\partial^2(\overline{x^\alpha u})/\partial t^2\}_{i+1/2}$$

in $\langle\overline{x^\alpha u}\rangle_{i+1/2}$, the errors of the order $O\{(\Delta t)^2\}$ in the bracketed term cancel and the resulting formula for updating $\bar{\Delta}V$ is perfectly valid. However, it does not reduce to the exact least-squares formula in the case of constant coefficients; in fact, it does not even lead to an upstream-centered scheme. In consequence, it even yields larger phase errors than interface differencing. The numerical results of Sec. 4 were still obtained with $\bar{\Delta}V$ updated according to (B4).

The most promising way to introduce least-squares fitting into the Lagrangean step seems to be by actual least-squares fitting of the final Lagrangean distribution, in some practical approximation. This has not yet been implemented to full satisfaction.

An alternative way to achieve least-squares accuracy is to start from initial-value distributions that are quadratic in each zone and continuous at the interfaces. The initial values hence are of the form

$$Q(t^0, \xi) = \bar{Q}_{i+1/2} + \{(Q_{i+1} - Q_i)/\Delta_{i+1/2}\xi\}(\xi - \bar{\xi}_{i+1/2}) + 3\{(Q_{i+1} - 2\bar{Q}_{i+1/2} + Q_i)/(\Delta_{i+1/2}\xi)^2\}\{(\xi - \bar{\xi}_{i+1/2})^2 - \tfrac{1}{12}(\Delta_{i+1/2}\xi)^2\}, \quad \xi_i \leqslant \xi \leqslant \xi_{i+1}. \tag{B5}$$

In [2] it was shown that the convective scheme V, based on the above zonewise initial-value distribution, has the same dispersive and dissipative evolutionary errors as scheme III, with a zonewise linear initial-value distribution obtained by least-squares fitting.

Using the quadratic distribution in the Lagrangean scheme means that the step of resolving the initial discontinuity at an interface drops out, while the formulas for the first time derivatives at an interface ξ_i become the usual characteristic equations (18)

and (19). Only in calculating the second time derivative one may (or may not) account for the discontinuity of first derivatives across characteristics departing from (t^0, ξ_i).

The apparent simplicity, however, is lost when the scheme is made monotonic or extended to two dimensions through time splitting. Under those circumstances the continuity of the state quantities at the interfaces must be given up. This scheme therefore has not yet been implemented for the equations of ICF.

ACKNOWLEDGMENTS

I thank Paul Woodward (Leiden Observatory and Lawrence Livermore Laboratory) for his great support in developing the multi-dimensional Euler version of the method. The idea of a separate remap step was his, as well as the enormous amount of energy spent in writing the MUSCL code. Without these, the multi-dimensional version of the method would still be on the drawing board.

REFERENCES

1. S. K. GODUNOV, *Mat. Sb.* **47** (1959), 271; also: Cornell Aeronautical Lab. Transl.
2. B. VAN LEER, *J. Computational Physics* **23** (1977), 276.
3. J. P. BORIS, U.S. Naval Research Lab. Memorandum Report 2542, December 1972.
4. S. K. GODUNOV, A. W. ZABRODYN, AND G. P. PROKOPOV, *Z. Vyčisl. Mat. i Mat. Fiz.* **1** (1961), 1020; also: Cornell Aeronautical Lab. Transl.
5. B. VAN LEER, *J. Computational Physics* **23** (1977), 263.
6. W. G. STRANG, *SIAM J. Numer. Anal.* **5** (1968), 506.
7. W. F. NOH AND P. R. WOODWARD, *in* "Lecture Notes in Physics No. 59," p. 330, Springer-Verlag, Berlin, 1977.
8. P. R. WOODWARD, private communication, 1977.
9. W. J. WEBER, J. P. BORIS, AND J. GARDNER, ALFVEN, a two-dimensional SHASTA code solving the radiative, diffusive MHD equations, *Comput. Phys. Comm.* **16** (1979), 243.
10. J. P. BORIS, U. S. Naval Research Lab. Memorandum Report 3237, March 1976.
11. J. E. FROMM, *J. Computational Physics* **3** (1968), 176.
12. B. VAN LEER, *in* "Lecture Notes in Physics No. 18," p. 163, Springer-Verlag, Berlin, 1973.
13. B. VAN LEER, *J. Computational Physics* **14** (1974), 361.
14. R. COURANT, E. ISAACSON, AND M. REES, *Comm. Pure Appl. Math.* **5** (1952), 243.
15. R. COURANT AND K. O. FRIEDRICHS, "Supersonic Flow and Shock Waves," Interscience, New York, 1948.
16. P. R. WOODWARD, private communication, 1978.
17. B. VAN LEER, The characteristic equations for discontinuous flow, appendix to original version of present paper, October 1977.
18. G. A. SOD, *J. Computational Physics* **27** (1978), 1.
19. R. D. RICHTMYER AND K. W. MORTON, "Difference Methods for Initial-Value Problems," 2nd ed., Interscience, New York, 1967.
20. J. E. FROMM, IBM Research Report RJ 780, 1970.